RESIDUAL STRESSES IN FINE GRINDING

By
S. BALAIAH

ME
1978
M
BAL
RES

TH
ME/1978/M
B181r

DEPARTMENT OF MECHANICAL ENGINEERING
INDIAN INSTITUTE OF TECHNOLOGY KANPUR
JULY, 1978

RESIDUAL STRESSES IN FINE GRINDING

A Thesis Submitted
In Partial Fulfilment of the Requirements
for the Degree of
MASTER OF TECHNOLOGY

By
S. BALAIAH

to the

DEPARTMENT OF MECHANICAL ENGINEERING
INDIAN INSTITUTE OF TECHNOLOGY KANPUR
JULY, 1978

ME-1972-M-PAN-NEW

CENTRAL LIBRARY
Acc. No. 54913

21 AUG 1978

In fond memory of my aunt,
who was my guardian.

CERTIFICATE

This is to certify that the thesis entitled "Residual Stresses in Fine Grinding" by S. Balaiah is a record of work carried out under my supervision and has not been submitted elsewhere for a degree.

Dr. G.K. Lal
Professor
Department of Mechanical Engineering
Indian Institute of Technology
Kanpur

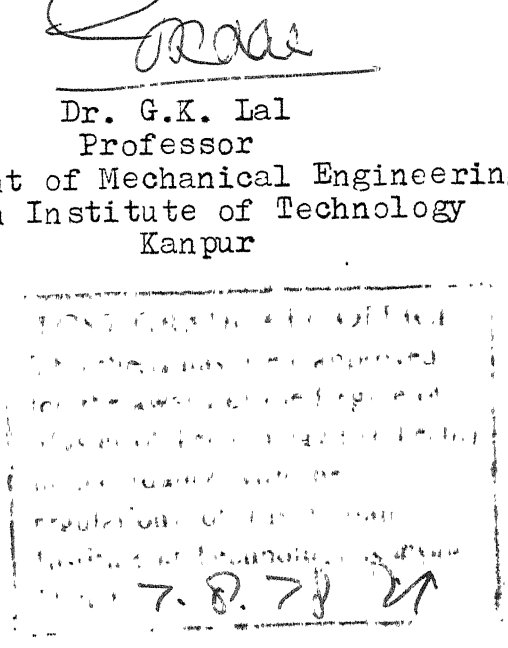

ACKNOWLEDGEMENTS

I express my deep sense of gratitude to Dr. G.K.Lal, my thesis supervisor, who created in me constant inspiration through his valuable suggestions and constructive criticism throughout this work.

I thank all of my friends who have made my stay at I.I.T. Kanpur pleasant. I am thankful to Dr. S.S. Rao for his valuable suggestions, and Mr. S.N. Sinha, Lecturer, Bihar College of Engineering, Patna, for the timely help rendered to me. My thanks are due to Mr. K.N. Tewari for flawless type writing.

Last but not the least I owe thanks to Sushee and Kalyani, my wife and daughter, for the patience shown throughout this work.

CONTENTS

LIST OF TABLES

LIST OF FIGURES

NOMENCLATURE

$A^{(e)}$	Element area
a_1, a_2 etc.	Constants in equation (4.2)
a_{A1}, a_{A2}, a_{A3}	Variables used in equation (A.5)
B	Workpiece width
b	Fictitious parameters used in equation (4.5).
b_{A1}, b_{A2}, b_{A3}	Constants used in equation (A.5)
b_c	Average width of the chip [Fig.4(b)]
b_G	Width of the surface heat source
C	Variable defined by the equation (3.16)
c	Number of active grains per unit contact area
c_o	Constant for a given wheel [Equation (2.4)]
D	Wheel diameter
[D]	Strain-stress transformation matrix
d	Wheel depth of cut
dA	Differential area
E	Elastic modulus of the workpiece material
F_p	Horizontal grinding force component
F_q	Vertical grinding force component
G	Shear modulus of the workpiece material
H	Non-dimensional convective coefficient of the grinding fluid [Equation (2.12)]
H_w	Warm hardness of the workpiece material
h	Dimensional convective coefficient of the grinding fluid

K	Thermal conductivity of the workpiece material
$[K]$	Assembled stiffness matrix
k	Thermal diffusivity of the workpiece material
$[k^{(e)}]$	Element stiffness matrix
$k^{(e)}_{ij}$	Element of the element stiffness matrix corresponding to ith row and jth column
L	Dimensionless half length of the heat source [Equation (2.12)]
ℓ	Half length of the heat source [Fig.(5)]
ℓ_c	Length of the chip [Fig.4(a)]
ℓ_G	Length of the surface heat source [Fig.4(b)]
ℓ_V	The distance by which the workpiece advances between two successive grains [Fig.4(a)]
M_c	Total number of grains in contact with the workpiece at any time
m_c	Constant for a given wheel [Equation (2.5)]
N	Matrix of shape functions
O	Origin of the coordinate system [Figs.(5,6)]
$\{P\}$	Assembled load vector
$\{p^{(e)}\}$	Element load vector
$p_i^{(e)}$	ith Element of the element load vector
$\dot{Q}_F$	Rate of total grinding energy generated
q_o	Characteristic heat source strength parameter
q_L	Strength of the line heat source
q_p	Strength of the point heat source
q_v	Strength of the volume heat source
q_{v_o}	Strength of the volume heat source at the surface.

R	Region of consideration [Fig.(5)]
r	Ratio of mean chipwidth to chip thickness
s	Ficticious parameter used in Equation (4.5)
T	Dimensional temperature
t	Maximum chip thickness
t'	Instantaneous chip thickness
t_o	Constant for a given wheel [Equation (2.4)]
t_1	Constant for a given wheel [Equation (2.5)]
U	Non-dimensional time
U_{ss}	Non-dimensional time required for a point in the workpiece to reach 99.99% of its maximum temperature
u	Displacement component along x coordinate axis [Fig.(5)]
V_s	Wheel speed
V_w	Table speed
v	Displacement component along y coordinate axis [Fig.(5)]
v'	Velocity of the moving heat source
w	Displacement component along z coordinate axis
X	Non-dimensional x coordinate [Equation (2.12)]
x	x-coordinate of a point in the workpiece
x'	x-coordinate of a point heat source
Y	Non-dimensional y coordinate
y	y-coordinate of a point in the workpiece
y'	y-coordinate of the point heat source
z	z-coordinate of a point in the workpiece
α	The fraction of total grinding energy entering the workpiece
α_1	The fraction of the total grinding energy entering the workpiece through the surface

α_2	The fraction of the total grinding energy generated in the workpiece due to deformation of the material
α_t	Thermal coefficient of linear expansion for the workpiece material
β	Decay coefficient for the volume heat source
$\gamma_{xy}, \gamma_{yz}, \gamma_{xz}$	Shear strains
$\varepsilon_x, \varepsilon_y, \varepsilon_z$	Normal strains along x,y,z axes,respectively
τ	Time variable
$\tau_{xy}, \tau_{yz}, \tau_{xz}$	Shear stresses corresponding to γ_{xy}, γ_{yz}, γ_{xz} respectively
$\sigma_x, \sigma_y, \sigma_z$	Normal stresses along x,y,z axes,respectively
η	Non-dimensional decay coefficient
ϕ	Non-dimensional temperature
ψ	Thermo elastic displacement potential
ν	Poisson ratio for the workpiece material
λ	Constant for a given material
ρ	Radius of the plastic zone
∇	Laplacian operator
θ	Variable representing sum of the normal stresses.

SYNOPSIS

RESIDUAL STRESSES IN FINE GRINDING

S. BALAIAH

MASTER OF TECHNOLOGY
Department of Mechanical Engineering
Indian Institute of Technology, Kanpur

In the present work an attempt has been made to evaluate the residual grinding stresses theoretically. Finite element method has been used to predict the distribution of residual stresses in the workpiece along the longitudinal as well as transverse direction during plunge-cut surface grinding. For simplicity only single pass grinding has been considered. Since the residual stresses are due to non-uniform thermal expansion of the workpiece, the temperature distribution in the workpiece during grinding has been evaluated following the model proposed by Sauer (9) with minor modifications.

The theoretical results indicate that the peak residual tensile stress in the workpiece may reach the ultimate strength of the workpiece resulting in thermal failure of the workpiece. The results also indicate that grinding conditions have significant effect on the residual stress distribution. The peak residual tensile stress appears to decrease with decreasing wheel speed and increasing table speed, while increasing depth of cut increases its magnitude. The convective property of the grinding fluid also appears to have significant effect on the residual stress distribution. These results qualitatively agree with the published experimental results.

CHAPTER 1

INTRODUCTION

In grinding, the material is removed by the action of many small cutting points of abrasive grains of unindentified geometry which are held together in the grinding wheel by some bond material. Considering the action of the grain [Fig.(1)] it was shown (6) that at the beginning of the interference zone [Fig.(2)] , where a grain first contacts the workpiece surface, sliding and ploughing occur. At this location forces are not sufficiently large to remove the material. As the grain moves along the workpiece, it encounters a thicker layer of uncutmaterial, forces increase and chip is removed. At the same time heat is generated at the grain-workpiece interface because of frictional sliding. Heat is also generated in the workpiece material because of plastic deformation. As the chip travels up the rake (leading) face of the grain heat is generated at the grain-chip interface. In adition to the temperature in the region of chip formation, the finished workpiece is also subjected to the wheel-workpiece interference zone temperature, as a result of this grinding burn or thermal cracks sometimes appear on the workpiece surface.

When any process which changes the shape or volume of an object in a non-uniform manner, the individual elements of the object undergo different changes in their dimensions. Besides the forces in the workpiece which are in equilibrium with the applied forces, additional forces maintain the equilibrium within the workpiece or object after the release of external loadings. These internal forces cause stresses which are called "Residual stresses" or "Locked-in stresses". These stresses are maximum at or near the surface. Such a stress produces distortion, thus creating a compensating stress or resisting stress in other parts of the object. Since it is usually widely distributed, the compensating stress is much lower in magnitude than the primary residual stress and is therefore not significant. Once formed, the stresses remain unchanged indefinitely unless relieved by plastic deformation or by failure.

The basic causes of residual stresses are,

(1) Structural transformation and consequent specific volume changes of micro-constituents in the workpiece.

(2) Mechanical forces at the wheel-workpiece interface giving rise to inhomogeneous elastic-plastic deformation of the workpiece.

(3) Inhomogeneous thermal expansion of the workpiece resulting in thermal stresses.

Under ordinary grinding conditions, the maximum temperature experienced by the workpiece will be well below the

structural allotropic transformation temperature of the work-piece (9). So the possibility of residual stresses being generated due to allotropic transformation is negligible. Secondly, the investigation carried out by Mishra, etal.(25) reveals that the mechanical forces that are involved in surface grinding bear insignificant effect on the residual stress distribution. In the light of above facts it becomes evident that the residual stresses in grinding are nothing but the thermal stresses.

A typical subsurface temperature distribution in the workpiece for plunge-cut surface grinding is shown in Fig.(3). At any point below the surface the product (temperature x thermal coefficient of expansion x elastic modulus of the material) gives a good estimate of the resulting instantaneous compressive stress. Because of the colder underlying material restraining free expansion, the compressive stresses build-up as temperature rises. When the compressive yield strength is exceeded plasticflow occurs causing upward flow on the free surface. After the material is returned to its average temperature the surface layer which had yielded is subjected to residual tensile stresses. The more the thermal upset, the higher is the magnitude of the residual stresses generated.

It is well established that the effect of residual stresses have a similar effect on the fatigue behaviour of

materials as do mechanically imposed static stresses of the same magnitude. Thus significant residual stresses are beneficial if compressive and detrimental if tensile, particularly in hardened materials. Thus for optimum design conditions, the control of residual stresses becomes an important factor in the control of fatigue strength of the component. Since the grinding operation is usually the last machining operation the analysis of residual grinding stresses becomes a relevant and a useful factor.

1.1 PREVIOUS WORK:

1.1.1 Grinding Temperatures:

Temperature distribution in the region of interest is necessary for the calculation of thermal stresses. Several researchers in the past (1-5) have attempted to measure the temperature distribution in the workpiece during grinding. Because of the difficulties associated with grinding temperature measurement, attempts (6-9) have been made to evaluate the temperature distribution analytically. These temperature models employ the theory of moving heat sources proposed by Jaeger (10). The investigation carried out by DesRuisseaux and Zerkle (6) considers temperature in the viscinity of chip-formation and relates this temperature to the temperature experienced by the workpiece after grinding. The relation is established by considering the grinding geometry. Malkin and Anderson (7) divided the total grinding energy into chip

formation, ploughing, and sliding energy components. Their results indicate that virtually all the sliding and ploughing energies, and approximately 55% of the chip formation energy are conducted as heat into the workpiece. Both these models have drawbacks in the sense that they do not take into account of the grinding fluid and the temperature rise due to the plastic-deformation of the workpiece material.

The thermal model proposed by Sauer (9) on the other hand determines the workpiece temperature during grinding by combining experimental and analytical techniques. Some of the parameters have been evaluated by comparing theoretical and experimental results so that the best possible agreement between both temperatures is obtained. The cooling ability of the grinding fluid and the temperature rise due to plastic deformation are also evaluated.

1.1.2 Residual Stresses:

Several researchers (12-26) in the past have attempted to explain the origin of the subsurface residual stresses which result from the grinding of metals. The magnitude of these stresses have been measured by the experimental techniques such as parting out method, Layer removal method, Hole drilling method, X-ray diffraction method, Ultrasonic method (26) etc., in an attempt to reduce the incidence of fatigue cracks in engineering components.

Although there are numerous experimental results available on grinding stresses, very few attempts were made to evaluate these stresses theoretically (23-25). Nokano, etal. (24), have shown that workpiece is deformed into convex shape during grinding because of the temperature difference between the top and bottom surfaces, and that the profile of finished workpieces become concave. The residual stress distribution in the workpiece due to surface grinding has been obtained analytically by Mishra, etal.(25). In this work the temperature distribution in the workpiece was calculated for the case of strip heat source moving on the surface of a semi-infinite body. Finite element method was applied to evaluate the residual stress distribution following the initial strain method. No attempt was made to evaluate the effect of grinding variables on the residual stress distribution, or to establish the validity of their model with experiments.

1.2 PRESENT WORK:

In the present work an attempt has been made to evaluate the residual grinding stresses theoretically.It has already been established that the residual stresses in the workpiece are due to the thermal stresses. In order to evaluate the temperature distribution in the workpiece during grinding, the model proposed by Sauer (9) has been adapted with minor changes. This model includesthe effect of grinding

fluid and plastic deformation and appears to yield results which are satisfactory. A computer program has been developed to evaluate the temperature numerically. The data used were those given in reference (9).

Finite element method has been used to evaluate the residual grinding stresses along the longitudinal and transverse direction during plunge-cut surface grinding. Subparametric constant strain triangular elements (CST) were used. The analysis has been used to predict the effect of various grinding conditions on the residual stress distribution. The results have been qualitatively compared with the experimental results published earlier.

CHAPTER 2

GRINDING TEMPERATURES

2.1 INTRODUCTION:

In recent years several attempts have been made to analyse the mechanics of chip formation with single abrasive grains. The model that appears to be most acceptable is the identation type model [Fig.4(b)] proposed by Shaw,etal (2, 30,31,32). They have obtained the average chip size and shape [Fig.4(a)] from the considerations of volume continuity. It was further assumed that the grain tips are conical in shape which appears to be justified on the basis of available experimental results with single abrasive grains (31,32). Their equations for the length of the chip, ℓ_c, the average width, b_c, and the maximum chip thickness, t, of an average chip are given by

$$\ell_c = \sqrt{Dd} \qquad (2.1)$$

$$b_c = \tfrac{1}{2} rt = \frac{V_w}{V_s} \frac{r}{c} \sqrt{\frac{d}{D}} \qquad (2.2)$$

$$t = \frac{4V_w}{V_s c r} \sqrt{\frac{d}{D}} \qquad (2.3)$$

where D is the wheel diameter, d is the wheel depth of cut, V_w is the workspeed, V_s is the wheel speed, c is the number of active grains per unit area and r is the ratio of mean chip width to mean chip thickness.

The variables c and r characterise the condition of the cutting surface of the wheel. Detailed discussion regarding these variables can be found in reference (34). Nakayama and Shaw (30) have approximated the measured values of c by the equation,

$$c = c_o(t - t_o) \tag{2.4}$$

where c_o and t_o are constants for a given wheel. Sauer (9) has suggested this relationship in the following form

$$c = \left(\frac{t}{t_1}\right)^{m_c} \tag{2.5}$$

where t_1, m_c are constants for a given wheel. His evaluated values of these constants are given in Table 2 while the values of r are given in Table 3.

The important factor in evaluating the grinding temperature is that a large amount of heat energy is generated deep in the workpiece due to plastic deformation that occurs beneath the grain. This heat source is called the "volume heat source". The detailed study of this aspect has been carried out by Sauer (9). In the present work his model and results have been extensively used for evaluating the temperature rise in the workpiece during grinding

The strength of the volume heat source, q_v, can be assumed to be an exponential function of the depth below the surface, y, of the form (9)

$$q_v = q_{v_o} e^{-\beta y} \qquad (2.6)$$

where q_{v_o} is the strength of the volume heat source at the surface ($y = 0$). The value of the decay coefficient, β, has to be determined experimentally. Sauer (9) has evaluated its value experimentally for AISI 1018 Cr steel and found it to be 27.73 1/in.

In addition to this volume heat source there will be heat sources acting at the wheel-work interface and at the chip-work interface, both of these sources are called "surface heat sources". The plane over which these heat sources extend is shown by the line B'C' in Fig. [4(b)]. Its width, b_G, equals the width of the chip, b_c, and the length is represented by ℓ_G and is equal to B'C'. Thus,

$$b_G = b_c \qquad (2.7)$$

The approximate relation for ℓ_G is given by (9)

$$\ell_G = 3.38 \sqrt{\frac{F_p}{M_c \pi H_w}} \frac{t'}{t} \qquad (2.8)$$

where F_p is the horizontal component of grinding force, M_c is the total number of grains in contact with the workpiece at any time, H_w is the warm hardness of the workpiece material and t' is the instantaneous chip thickness. Approximating the chip shape to be a slender wedge (6) instantaneous chip thickness, t', can be evaluated from

$$t' = \frac{(x + \ell_c)}{2\,\ell_c}\, t \qquad (2.9)$$

where x is the horizontal location of the maximum chip thickness from the origin O. [Figs.(5,6)].

2.2 ANALYSIS:

The workpiece can be represented mathematically by a region R as shown in Fig.(5).

$$R = \begin{vmatrix} -\infty < x < \infty \\ -\infty < z < \infty \\ 0 \leq y < \infty \end{vmatrix} \qquad (2.10)$$

The area of contact between the workpiece and the wheel is from $x = -\ell$ to $x = \ell$ and infinitely far in the z direction. Thus we can assume that there is no temperature variation in the z direction when the workpiece moves with the constant velocity V_w relative to the stationary wheel in negative x direction. The coordinate system is fixed to the wheel having O as the origin as shown in Fig.(6). Since the depth of cut, d, is much smaller than the length of contact, the plane ABOCD can be approximated as y = 0 plane.

The model of a semi-infinite body can be used to simulate the finite body if the body is large enough so that end effects can be neglected at the centre portion of the body and the actual temperature distribution can be approximated by the steady state temperature distribution.

2.2.1 Temperature Field in a Semi-infinite Solid due to Moving Sources of Heat:

The equations for calculating the temperature distribution in the workpiece during surface grinding have been simplified by Sauer (9). In deriving these equations, the theory of moving heat sources for the case of line heat source proposed by Jaeger (11) has been used.

The steady state temperature distribution in the semi-infinite body due to moving line heat source of strength q_L can be evaluated from (11) as

$$T_L(x,y) = \left[\frac{q_L}{\rho c}\int_0^{\infty} \exp\left\{\frac{-(x-x'+v'\tau)^2}{4k\tau}\right\}\left[\frac{\exp\left\{\frac{-(y-y')^2}{4k\tau}\right\}}{4\pi k\tau} + \frac{\exp\left\{\frac{-(y+y')^2}{4k\tau}\right\}}{4\pi k\tau}\right] d\tau\right] - \left[\frac{q_L}{2\rho c}\int_0^{\infty} \frac{h/K}{\sqrt{\pi k\tau}}\right.$$

$$\left.\operatorname{erfc}\left\{\frac{y+y'+2\frac{h}{K}k\tau}{2\sqrt{k\tau}}\right\} \exp\left\{(y+y')\frac{h}{K} + k\left(\frac{h}{K}\right)^2\tau\right.\right.$$

$$\left.\left. - \frac{(x-x'+v'\tau)^2}{4k\tau}\right\} d\tau\right] \qquad (2.11)$$

$$q_p = q_L\, dz'\, d\tau'$$

where x', y', z' are the coordinates of the point source of strength q_p acting at time τ', ρ is the extent of the plastic zone as shown in Fig.(4(a)), v' is the velocity of

the heat source, k is the thermal diffusivity of the work-piece material, K is the thermal conductivity of the work-piece material and h is the convective coefficient of the cooling medium.

Sauer (9) has simplified the above equation by introducing the following non-dimensional quantities,

$$
\begin{aligned}
X &= \frac{v'}{2k}\, x \\
Y &= \frac{v'}{2k}\, y \\
U &= \frac{v'^2}{2k}\, \tau \\
H &= \frac{h}{K}\ \frac{2k}{v'} \\
\phi &= \frac{\pi\ K\ v'}{2q_o}\, T \\
L &= \frac{v'}{2k}\ \frac{\ell}{2}
\end{aligned}
\qquad (2.12)
$$

where X is the dimensionless x coordinate, Y is the dimensionless y coordinate, U is the dimensionless time variable, H is the dimensionless convective coefficient, ϕ is the dimensionless temperature, L is the dimensionless half length of the heat source, T is the temperature variable and q_o is the source strength parameter. Equation (2.11) thus takes the form,

$$\phi_L = \frac{q_L}{q_o}\frac{v'}{8k}\int_o^\infty \exp\left\{\frac{-(X-X'+U)^2}{2U}\right\}\left[\exp\left\{\frac{-(Y-Y')^2}{2U}\right\}\right.$$

$$\left. + \exp\left\{\frac{-(Y+Y')^2}{2U}\right\}\right]\frac{dU}{U} - \frac{q_L}{q_o}\frac{v'H}{4k}\sqrt{\frac{\pi}{2}}$$

$$\int_o^\infty \operatorname{erfc}\left\{\frac{Y+Y'+HU}{\sqrt{2U}}\right\} \exp\left\{\frac{-(X-X'+U)^2}{2U}\right\} \exp\left\{H(Y+Y')+\frac{H^2U}{2}\right\}\frac{dU}{\sqrt{U}}$$

(2.13)

This equation can be considered in two parts, the first part representing the temperature rise due to the heat source without convective loss from the surface and the second part representing the temperature reduction due to convective cooling from the surface.

2.2.1(a) Temperature Rise due to Single Grain Surface Heat Source:

Assuming the strength of the heat source, q_L, to be uniform over its length, we get

$$q_L = q_o\, dx' \qquad \text{for } -\ell \le x' \le \ell \;;\; y' = 0 \qquad (2.14)$$

Integrating the first part of equation (2.13) over the extent of the heat source, the temperature rise, ϕ_1, will be

$$\phi_1 = \tfrac{1}{2}\sqrt{\frac{\pi}{2}}\int_o^\infty \frac{\exp(-\frac{Y^2}{2U})}{\sqrt{U}}\left\{\operatorname{erfc}\left(\frac{X-L+U}{\sqrt{2U}}\right) - \operatorname{erfc}\left(\frac{X+L+U}{\sqrt{2U}}\right)\right. dU$$

(2.15)

2.2.1(b) Temperature Rise due to Single Grain Volume Heat Source:

The strength of the volume heat source can be evaluated from (9) as

$$q_L = q_o \beta e^{-\beta y'} dy' dx' \qquad \text{for } -\ell \leq x' \leq \ell, \quad 0 \leq y' < \infty \qquad (2.16)$$

where β is the decay coefficient. Introducing the dimensionless decay coefficient, η, as defined by

$$\eta = \frac{2k}{v'} \beta$$

and after integrating the first part of equation (2.13) over the extent of heat source the temperature rise due to volume heat source, ϕ_2, is given by

$$\phi_2 = \frac{\pi\eta}{8} \int_0^\infty \{ \operatorname{erfc}\left(\frac{X-L+U}{\sqrt{2U}} \right) - \operatorname{erfc}\left(\frac{X+L+U}{\sqrt{2U}} \right) \}$$

$$\exp\left(\eta^2 \frac{U}{2} \right) \{ \exp(\eta Y) \operatorname{erfc}\left(\frac{\eta U+Y}{\sqrt{2U}}\right)$$

$$+ \exp(-\eta Y) \operatorname{erfc}\left(\frac{\eta U-Y}{\sqrt{2U}}\right) \} \, dU \qquad (2.17)$$

2.2.1(c) Temperature Rise due to Interference Zone Surface Heat Source:

Assuming the surface heat source, q_L, to be linearly varying with x', we get

$$q_L = q_o\left(1 + \frac{x'}{\ell}\right) dx' \qquad \text{for} \quad -\ell \le x' \le \ell$$
$$y' = 0 \qquad (2.18)$$

After integrating the first part of equation (2.13) over the extent of heat source, the temperature rise due to interference zone surface heat source, ϕ_3, is

$$\phi_3 = \frac{1}{2L}\int_0^\infty \exp\left(-\frac{Y^2}{2U}\right)\left[\sqrt{\frac{\pi}{2U}}(X+L+U)\left\{\operatorname{erfc}\left(\frac{X-L+U}{\sqrt{2U}}\right)\right.\right.$$
$$\left.\left. - \operatorname{erfc}\left(\frac{X+L+U}{\sqrt{2U}}\right)\right\} + \left\{\exp\left(\frac{-(X+L+U)^2}{2U}\right) - \exp\left(\frac{-(X-L+U)^2}{2U}\right)\right\}\right] dU$$
$$(2.19)$$

Temperature reduction due to surface cooling:

After integrating the second part of equation (2.13) over the extent of the heat source, the reduction in temperature, ϕ_5, due to surface cooling is given by

$$\phi_5 = \frac{\pi H}{4L}\int_0^\infty \exp\left(HY + \frac{H^2U}{2}\right)\operatorname{erfc}\left(\frac{Y+HU}{\sqrt{2U}}\right)\left[(X+L+U)\left\{\operatorname{erfc}\left(\frac{X-L+U}{\sqrt{2U}}\right)\right.\right.$$
$$\left.\left. - \operatorname{erfc}\left(\frac{X+L+U}{\sqrt{2U}}\right)\right\} + \sqrt{\frac{2U}{\pi}}\left\{\exp\left(\frac{-(X+L+U)^2}{2U}\right) - \exp\left(\frac{-(X-L+U)^2}{2U}\right)\right\}\right] dU$$
$$(2.20)$$

Hence the effective temperature rise due to interference zone surface heat source is given by

$$\phi_{3,5} = \phi_3 - \phi_5$$

2.2.1(d) Temperature Rise due to Interference Zone Volume Heat Source:

The source strength is assumed to be linearly varying with x' so that

$$q_L = \beta q_o (1 + \frac{x'}{\ell})\, e^{-\beta y'}\, dx'\, dy' \quad \text{for} \quad -\ell \leq x' \leq \ell, \quad 0 \leq y' < \infty \tag{2.21}$$

After integrating the first part of equation (2.13) over the extent of the heat source, the temperature rise, ϕ_4, due to interference zone volume heat source is

$$\phi_4 = \frac{\pi\eta}{8L} \int_0^\infty \exp(\frac{\eta^2 U}{2}) \left[\exp(\eta Y)\, \operatorname{erfc}(\frac{\eta U + Y}{\sqrt{2U}}) + \exp(-\eta Y)\, \operatorname{erfc}(\frac{\eta U - Y}{\sqrt{2U}})\right] \left[(X + L + U) \left\{\operatorname{erfc}(\frac{X-L+U}{\sqrt{2U}}) - \operatorname{erfc}(\frac{X+L+U}{\sqrt{2U}})\right\} + \sqrt{\frac{2U}{\pi}} \left\{ \exp(\frac{-(X+L+U)^2}{2U}) - \exp(\frac{-(X-L+U)^2}{2U})\right\} \right] dU \tag{2.22}$$

Temperature reduction due to surface cooling:

After integrating the second part of equation (2.13) over the extent of the heat source, the reduction in temperature, ϕ_6, due to surface cooling is given by

$$\phi_6 = \frac{\pi\eta}{4L} H \int_0^\infty [(X+L+U)\{\operatorname{erfc}(\frac{X-L+U}{\sqrt{2U}}) - \operatorname{erfc}(\frac{X+L+U}{\sqrt{2U}})\}$$

$$+ \sqrt{\frac{2U}{\pi}}\{\exp(\frac{-(X+L+U)^2}{2U}) - \exp(\frac{-(X-L+U)^2}{2U})\}$$

$$\{\frac{\exp(HY+\frac{H^2U}{2})}{\eta - H} \operatorname{erfc}(\frac{Y+HU}{\sqrt{2U}}) + \frac{\exp(\eta Y+\frac{\eta^2 U}{2})}{H-\eta}$$

$$\operatorname{erfc}(\frac{Y+\eta U}{\sqrt{2U}})\}]\, dU \qquad (2.23)$$

Thus, the effective temperature rise due to interference zone volume heat source will be

$$\phi_{4,6} = \phi_4 - \phi_6$$

and the overall temperature rise of the workpiece is

$$\phi = \phi_1 + \phi_2 + \phi_{3,5} + \phi_{4,6}$$

To obtain the dimensional temperature, T, the nondimensional temperature, ϕ , has to be multiplied by the factor

$$(\frac{2q_o k}{\pi K V_w})$$

The characteristic parameter, q_o, for different heat sources are (9)

$$q_{o(1)} = \frac{\alpha_1 \dot{Q}_F}{\ell_G b_G M_c}(1 + \frac{X}{L})$$

$$q_{o(2)} = \frac{\alpha_2 \dot{Q}_F}{\ell_G b_G M_c}(1 + \frac{X}{L})$$

$$q_{o(3,5)} = \frac{\alpha_1 \dot{Q}_F}{\ell_c B}$$

$$q_{o(4,6)} = \frac{\alpha_2 \dot{Q}_F}{\ell_c B} \qquad (2.24)$$

where α_1 is the fraction of the total grinding energy entering the workpiece through the surface ($y = 0$), α_2 is the fraction of the total grinding energy generated in the workpiece due to plastic deformation, $\dot{Q}_F$ is the rate of total grinding energy generated, and B is the work width.

$\alpha = \alpha_1 + \alpha_2$ and $\dot{Q}_F$ is given by

$$\dot{Q}_F = \frac{F_p V_s}{(12)(778)} \quad \text{Btu/sec.} \qquad (2.25)$$

The temperature so obtained is the steady state temperature over the ambient temperature.

In deriving the above equations the thermodynamic properties of the material of the semi-infinite region are assumed to be independent of the temperature variation. But for the real materials it is not true. However, comparison of temperature distribution with constant properties and with variable properties indicates no significant difference (9). Hence the average value of the material properties have been used in the present work.

As per the theories of hardness test (32), the warm hardness of the workpiece material has been taken as three times the yield stress of the workpiece material at its average temperature during grinding.

Using equations (2.13) through (2.22), the temperature rise can be evaluated. The details of the numerical technique used for evaluating this on computer is discussed later.

CHAPTER 3

RESIDUAL GRINDING STRESSES

3.1 INTRODUCTION:

As discussed earlier the residual stresses in grinding are the thermal stresses generated due to non-uniform thermal expansion of the workpiece. In the present work, the average values of the thermodynamic and mechanical properties of the workpiece material have been used and the material is assumed to be isotropic. The strain-stress relations for a three dimensional thermal stress problem of an isotropic solid are (36),

$$\varepsilon_x - \alpha_t T = \frac{1}{E}[\sigma_x - \nu(\sigma_y + \sigma_z)]$$

$$\varepsilon_y - \alpha_t T = \frac{1}{E}[\sigma_y - \nu(\sigma_x + \sigma_z)] \qquad (3.1(a))$$

$$\varepsilon_z - \alpha_t T = \frac{1}{E}[\sigma_z - \nu(\sigma_x + \sigma_y)]$$

$$\gamma_{xy} = \frac{\tau_{xy}}{G} \; ; \quad \gamma_{yz} = \frac{\tau_{yz}}{G} \; ; \quad \gamma_{xz} = \frac{\tau_{xz}}{G} \qquad (3.1(b))$$

where σ_x, σ_y, σ_z are the normal stresses along x, y, z axes of the coordinate system [Fig.(5)] , ε_x, ε_y, ε_z are the normal strains along x,y,z axes, τ_{xy},τ_{yz}, τ_{xz} are the shear stresses, γ_{xy}, γ_{yz}, γ_{xz} are the shear strains and ν , E, G, α_t are the poisson ratio, elastic modulus, shear modulus, thermal coefficient of linear expansion of the workpiece material

respectively. Equations(3.1(b)) are not affected by the temperature as free thermal expansion does not produce angular distortion in an isotropic material. The volume expansion, e, and the sum of the normal stresses, θ, are given by

$$e = \varepsilon_x + \varepsilon_y + \varepsilon_z$$
$$\theta = \sigma_x + \sigma_y + \sigma_z \tag{3.2}$$

e and θ are related by the equation,

$$e = \frac{(1 - 2\nu)}{E}\theta \tag{3.3}$$

Using equations (3.1(a)), (3.2) and (3.3), we get

$$e = \frac{1}{E}(1 - 2\nu)\theta + 3\alpha_t T \tag{3.4}$$

Thus, the stresses are

$$\sigma_x = \lambda e + 2G\varepsilon_x - \frac{\alpha_t E T}{1-2\nu}$$
$$\sigma_y = \lambda e + 2G\varepsilon_y - \frac{\alpha_t E T}{1-2\nu} \tag{3.5}$$
$$\sigma_z = \lambda e + 2G\varepsilon_z - \frac{\alpha_t E T}{1-2\nu}$$

where

$$\lambda = \frac{\nu E}{(1 + \nu)(1-2\nu)}$$
$$G = \frac{E}{2(1 + \nu)} \tag{3.6}$$

The equations of equilibrium for an elastic continuum without body forces are given by (36)

$$\begin{aligned}
\frac{\partial \sigma_x}{\partial x} + \frac{\partial \tau_{xy}}{\partial y} + \frac{\partial \tau_{xz}}{\partial z} &= 0 \\
\frac{\partial \sigma_y}{\partial y} + \frac{\partial \tau_{xy}}{\partial x} + \frac{\partial \tau_{yz}}{\partial z} &= 0 \\
\frac{\partial \sigma_z}{\partial z} + \frac{\partial \tau_{xz}}{\partial x} + \frac{\partial \tau_{yz}}{\partial y} &= 0
\end{aligned} \tag{3.7}$$

and the strain-displacement relations are

$$\begin{aligned}
\varepsilon_x = \frac{\partial u}{\partial x} \; ; \quad \varepsilon_y = \frac{\partial v}{\partial y} \; ; \quad \varepsilon_z = \frac{\partial w}{\partial z} \\
\gamma_{xy} = \frac{\partial u}{\partial y} + \frac{\partial v}{\partial x} \\
\gamma_{xz} = \frac{\partial u}{\partial z} + \frac{\partial w}{\partial x} \\
\gamma_{yz} = \frac{\partial v}{\partial z} + \frac{\partial w}{\partial y}
\end{aligned} \tag{3.8}$$

where u,v,w are the displacement components along x, y, z axes respectively. Using equations (3.1), (3.7) and (3.8), the equations of equilibrium can be expressed in terms of displacements as

$$\begin{aligned}
(\lambda + G) \frac{\partial e}{\partial x} + G \nabla^2 u - \frac{\alpha_t E}{1-2\nu} \frac{\partial T}{\partial x} &= 0 \\
(\lambda + G) \frac{\partial e}{\partial y} + G \nabla^2 v - \frac{\alpha_t E}{1-2\nu} \frac{\partial T}{\partial y} &= 0 \\
(\lambda + G) \frac{\partial e}{\partial z} + G \nabla^2 w - \frac{\alpha_t E}{1-2\nu} \frac{\partial T}{\partial z} &= 0
\end{aligned} \tag{3.9}$$

where $\nabla = \frac{\partial}{\partial x} + \frac{\partial}{\partial y} + \frac{\partial}{\partial z}$.

Any particular solution of equation (3.9) will reduce the thermal stress problem to an ordinary problem of surface forces. The solution for u,v,w, subject to the boundary conditions of a particular case will give, by means of equations (3.8) and (3.1), the values of the stress components of the corresponding problem. One way of finding particular solution to equation (3.9) is to take

$$u = \frac{\partial \psi}{\partial x} \quad ; \quad v = \frac{\partial \psi}{\partial y} \quad ; \quad w = \frac{\partial \psi}{\partial z} \tag{3.10}$$

where the thermoelastic displacement potential, ψ , is a function of x,y,z and also a function of time if temperature varies with time. Using equation (3.6), equations (3.9) can be rewritten in the form

$$\begin{aligned} \frac{\partial e}{\partial x} + (1-2\nu)\,\nabla^2 u &= 2(1+\nu)\,\alpha_t \frac{\partial T}{\partial x} \\ \frac{\partial e}{\partial y} + (1-2\nu)\,\nabla^2 v &= 2(1+\nu)\,\alpha_t \frac{\partial T}{\partial y} \\ \frac{\partial e}{\partial z} + (1-2\nu)\,\nabla^2 w &= 2(1+\nu)\,\alpha_t \frac{\partial T}{\partial z} \end{aligned} \tag{3.11}$$

Since $e = \frac{\partial u}{\partial x} + \frac{\partial v}{\partial y} + \frac{\partial w}{\partial z}$, equation (3.10) will yield

$$e = \nabla^2 \psi$$

and equation (3.11) becomes

$$(1-\nu)\frac{\partial}{\partial x}(\nabla^2 \psi) = (1+\nu)\,\alpha_t \frac{\partial T}{\partial x}$$

$$(1 - \nu) \frac{\partial}{\partial y} (\nabla^2 \psi) = (1 + \nu) \alpha_t \frac{\partial T}{\partial y} \qquad (3.12)$$

$$(1 - \nu) \frac{\partial}{\partial z} (\nabla^2 \psi) = (1 + \nu) \alpha_t \frac{\partial T}{\partial z}$$

Equations (3.12) are satisfied by taking the function ψ as a solution of the poisson's equation,

$$\nabla^2 \psi = \left(\frac{1 + \nu}{1 - \nu} \right) \alpha_t T \qquad (3.13)$$

Now any thermal stress problem can be solved by solving the above equation provided the temperature function; $T(x,y,z)$, is known.

3.2 ANALYSIS:

The temperature distribution in the workpiece during grinding, as discussed earlier, is independent of the z direction. Thus equation (3.13) can be further simplified to the plane-strain condition.

$$\frac{\partial^2 \psi}{\partial x^2} + \frac{\partial^2 \psi}{\partial y^2} = \left(\frac{1 + \nu}{1 - \nu} \right) \alpha_t T(x,y) \qquad (3.14)$$

Since the temperature distribution is evaluated numerically, numerical solution method has been used for evaluating thermal stresses also. The finite element method has been used for evaluating the thermal stresses since it yields better results than the finite difference method.

Solution of Poisson's equation by Finite element method:

The equation (3.14) can be written as

$$\frac{\partial^2 \psi}{\partial x^2} + \frac{\partial^2 \psi}{\partial y^2} + C = 0 \qquad (3.15)$$

where $C = -\left(\frac{1+\nu}{1-\nu}\right)\alpha_t T$ (3.16)

Equation (3.15) is the necessary condition for functional F to be minimum. This functional F, is given by (38)

$$F = \iint_R \left[\tfrac{1}{2}\left(\frac{\partial\psi}{\partial x}\right)^2 + \tfrac{1}{2}\left(\frac{\partial\psi}{\partial y}\right)^2 - C\psi\right] dx\, dy \qquad (3.17)$$

where R is the region of consideration [Fig.(5)]. Thus the solution, ψ, of equation (3.15) is that value of ψ which minimises the functional F [equation (3.17)]. Minimisation of the functional, F, and the equations for the element stiffness matrix and the load vector are clearly given in reference (38). Final form of these equations are

$$k_{ij}^{(e)} = \int_{A^{(e)}} \int \left(\frac{\partial N_i}{\partial x}\frac{\partial N_j}{\partial x} + \frac{\partial N_i}{\partial y}\frac{\partial N_j}{\partial y}\right) dA \qquad (3.18)$$

$$p_i^{(e)} = -\int_{A^{(e)}} C\, N_i\, dA \qquad (3.19)$$

where $k_{ij}^{(e)}$ and $p_i^{(e)}$ are the elements corresponding to ith row and jth column of the element stiffness matrix, $\{k^{(e)}\}$, and element load vector, $\{p^{(e)}\}$, respectively. N_i, N_j are shape functionsassociated with the nodes and $A^{(e)}$ is the element area. The assembled equation is

$$[K]\ \{\psi\} + \{P\} = 0 \qquad (3.20)$$

where [K] is the assembled stiffness matrix, $\{\psi\}$ is the solution vector of the nodal values of ψ, and $\{P\}$ is

the assembled load vector. The set of simultaneous equations (3.20) are solved by Gauss elimination method to obtain the solution vector, $\{\psi\}$, subject to the boundary conditions discussed below.

Boundary conditions:

Referring to Fig.(7), the workpiece in an actual surface grinding is fixed on the magnetic chuck. The experimental results that are available in the literature (21) reveal that the depth upto which the residual stresses are dominant is very low compared to the total depth of the workpiece. Hence, at depth, say $y = y_h$, in the material itself the displacements are very low. By trial and error method the depth y_h was found to be 0.14 in., where the displacements are insignificant compared to the displacements near the surface. This is achieved by prescribing the value of ψ to be zero at $y = y_h$. The displacements are computed and compared with the displacements in the upper region, i.e., $y < y_h$. It was found that the displacements at $y = 0.14$ in. were of the order of 10^{-11} to 10^{-9} whereas the displacements near the surface $y = 0$, were of the order of 10^{-3}.

The continuum is divided into subparametric triangular elements. A linear interpolation function is used for the description of the geometry and a quadratic interpolation function is used for the variation of ψ within the element.

A single degree of freedom system is sufficient to satisfy the boundary condition. The temperature distribution within the continuum is specified by giving as input the temperatures at each of the nodal points. The variation of ψ within the element, $\psi^{(e)}$, has been taken as

$$\psi^{(e)} = [N]\{\psi^{(e)}_{nodal}\} \tag{3.21}$$

Displacements:

The displacements are obtained from

$$\begin{bmatrix} u \\ v \end{bmatrix} = \begin{bmatrix} \frac{\partial \psi}{\partial x} \\ \frac{\partial \psi}{\partial y} \end{bmatrix} \tag{3.22}$$

where

$$\frac{\partial \psi}{\partial x} = \begin{bmatrix} \frac{\partial N_1}{\partial x} & \frac{\partial N_2}{\partial x} & \frac{\partial N_3}{\partial x} & \frac{\partial N_4}{\partial x} & \frac{\partial N_5}{\partial x} & \frac{\partial N_6}{\partial x} \end{bmatrix} \begin{bmatrix} \psi_1 \\ \psi_2 \\ \psi_3 \\ \psi_4 \\ \psi_5 \\ \psi_6 \end{bmatrix}$$

$$\frac{\partial \psi}{\partial y} = \begin{bmatrix} \frac{\partial N_1}{\partial y} & \frac{\partial N_2}{\partial y} & \frac{\partial N_3}{\partial y} & \frac{\partial N_4}{\partial y} & \frac{\partial N_5}{\partial y} & \frac{\partial N_6}{\partial y} \end{bmatrix} \begin{bmatrix} \psi_1 \\ \psi_2 \\ \psi_3 \\ \psi_4 \\ \psi_5 \\ \psi_6 \end{bmatrix} \tag{3.23}$$

Strains:

The strains are given by

$$\begin{Bmatrix} \varepsilon_x \\ \varepsilon_y \\ \gamma_{xy} \end{Bmatrix} = \begin{Bmatrix} \frac{\partial^2 \psi}{\partial x^2} \\ \frac{\partial^2 \psi}{\partial y^2} \\ 2\frac{\partial^2 \psi}{\partial x\, \partial y} \end{Bmatrix} \qquad (3.24)$$

For plane strain condition where $\frac{\partial^2 \psi}{\partial x^2}$, $\frac{\partial^2 \psi}{\partial y^2}$ are obtained by differentiating $\partial\psi/\partial x$, $\partial\psi/\partial y$ with respect to x and y, respectively in the same manner as $\partial\psi/\partial x$, $\partial\psi/\partial y$ are obtained from equation (3.21).

Stresses:

From the strain-stress relations given by equation(3.1), for the case of plane strain condition, the stress components can be expressed by

$$\{\sigma\} = \begin{Bmatrix} \sigma_x \\ \sigma_y \\ \tau_{xy} \end{Bmatrix} = [D] \{\{\varepsilon\} - \{\varepsilon_o\}\} \qquad (3.25)$$

where $\{\varepsilon\} = \begin{Bmatrix} \varepsilon_x \\ \varepsilon_y \\ \gamma_{xy} \end{Bmatrix}$ and $\{\varepsilon_o\} = (1+\nu) \begin{Bmatrix} \alpha_t T \\ \alpha_t T \\ 0 \end{Bmatrix}$

(3.26)

and

$$[D] = \frac{E(1-\nu)}{(1+\nu)(1-2\nu)} \begin{bmatrix} 1 & \nu/(1-\nu) & 0 \\ \nu/(1-\nu) & 1 & 0 \\ 0 & 0 & (1-2\nu) \end{bmatrix}$$

These stress components can also be obtained from equation (3.5). σ_z, the stress along the transverse direction is obtained from equation (3.5). The strains and the stresses are constant within the element.

The element stiffness matrix and element load vector are derived for the subparametric triangular element. These matrices along with the ψ-displacement and displacement-strain, transformation matrices are given in Appendix. Boundary conditions are incorporated by eliminating the rows and columns of the assembled stiffness matrix and the rows of the assembled load vector corresponding to the zero degrees of freedom.

Now having obtained the temperature distribution and using equation (3.14) thermal stresses can be evaluated numerically. The details of numerical method used for evaluating this on computer is discussed later.

CHAPTER 4

NUMERICAL SOLUTION

The computer program is divided in two parts. The first part calculates the grinding temperatures numerically. The temperature data so obtained are used as input to the second part to evaluate the thermal stresses.

Equations (2.15) through (2.23), which describe the steady state temperature distribution in the moving semi-infinite solid, cannot be integrated analytically. Hence to obtain numerical results for a specific problem, a general purpose computer program has been developed. The numerical integration is carried out by using 10 point Gaussian-quadrature. A standard subroutine is used for this purpose. The results so obtained are compared with the results given by Sauer (9). Good agreement is evidenced from Figs. (8 through 13). Since the computer is limited in size and the numbers which it can handle, two problems that arise in this solution method had to be overcome.

Some of the equations contain terms of the form

$$e^{(s^2-b^2)} \ \mathrm{erfc}(s) \qquad (4.1)$$

For large values of s (say > 9) the exponential part of the expression (4.1) increases rapidly beyond the limit of computer (10^{38} for IBM 7044), while the value of the complete

term remains finite for all possible values of s. Hence, the complenentary error function had to be approximated as

$$\operatorname{erfc}(s) = e^{-s^2} \sum_{i=1}^{5} \frac{a_i}{(1+p\,s)^i} \quad \text{for } s \geq 0 \qquad (4.2)$$

This is based on the formula given by Hastings (39). Here a_i and p are constants and have the values given below.

$$\begin{aligned} p &= 0.3275911 \\ a_1 &= 0.22583684 \\ a_2 &= -0.25212866 \\ a_3 &= 1.25969513 \\ a_4 &= -1.28782245 \\ a_5 &= 0.94064607 \end{aligned} \qquad (4.3)$$

Using equations (4.2) and (4.3), expression (4.1) can be calculated by defining a new function,

$$\operatorname{experf}(s) = e^{s^2} \operatorname{erfc}(s) = \sum_{i=1}^{5} \frac{a_i}{(1+ps)^i} \quad \text{for } s \geq 0 \qquad (4.4)$$

Thus,

$$e^{(s^2-b^2)} \operatorname{erfc}(s) = e^{-b^2} \operatorname{experf}(s) \qquad (4.5)$$

where s and b are related such that

$$s^2 < b^2 \quad \text{for } s < 0 \qquad (4.6)$$

The new function is not defined for negative value of S but this is not necessary. Hence both parts of expression (4.1) remain constant for all finite values of s.

The second problem faced during computation was due to the definition of finite upper limit for the integration of equations (2.15) through (2.23). The upper limit ∞ implies that the calculated temperature is steady state temperature. However, this amounts to saying that the upper limit of integration is the time, say U_{ss}, at which the point of the coordinate system has reached its 99.99% of the maximum temperature. This time, U_{ss}, is a function of the half length of the heat source,L, and the position of the point in the coordinate system. The expression for U_{ss} as given by Sauer (9) has been used in the present program.

$$U_{ss} = 2L - X + 0.5Y + 10 \qquad (4.7)$$

Thus the steady state temperature distribution has been obtained by using U_{ss} as the upper limit of integration. For time less than U_{ss}, transient temperature field can be calculated.

The second part of the program calculates the thermal stresses numerically using equation (3.14) by employing the finite element method. For checking the correct assemblage of the assembled stiffness matrix and the total load vector etc., a sample problem with 4 elements was solved and the results obtained were checked with hand calculations.

The flowcharts for both part one and part two of the computer program are given in Figs.(N.1) and (N.2).

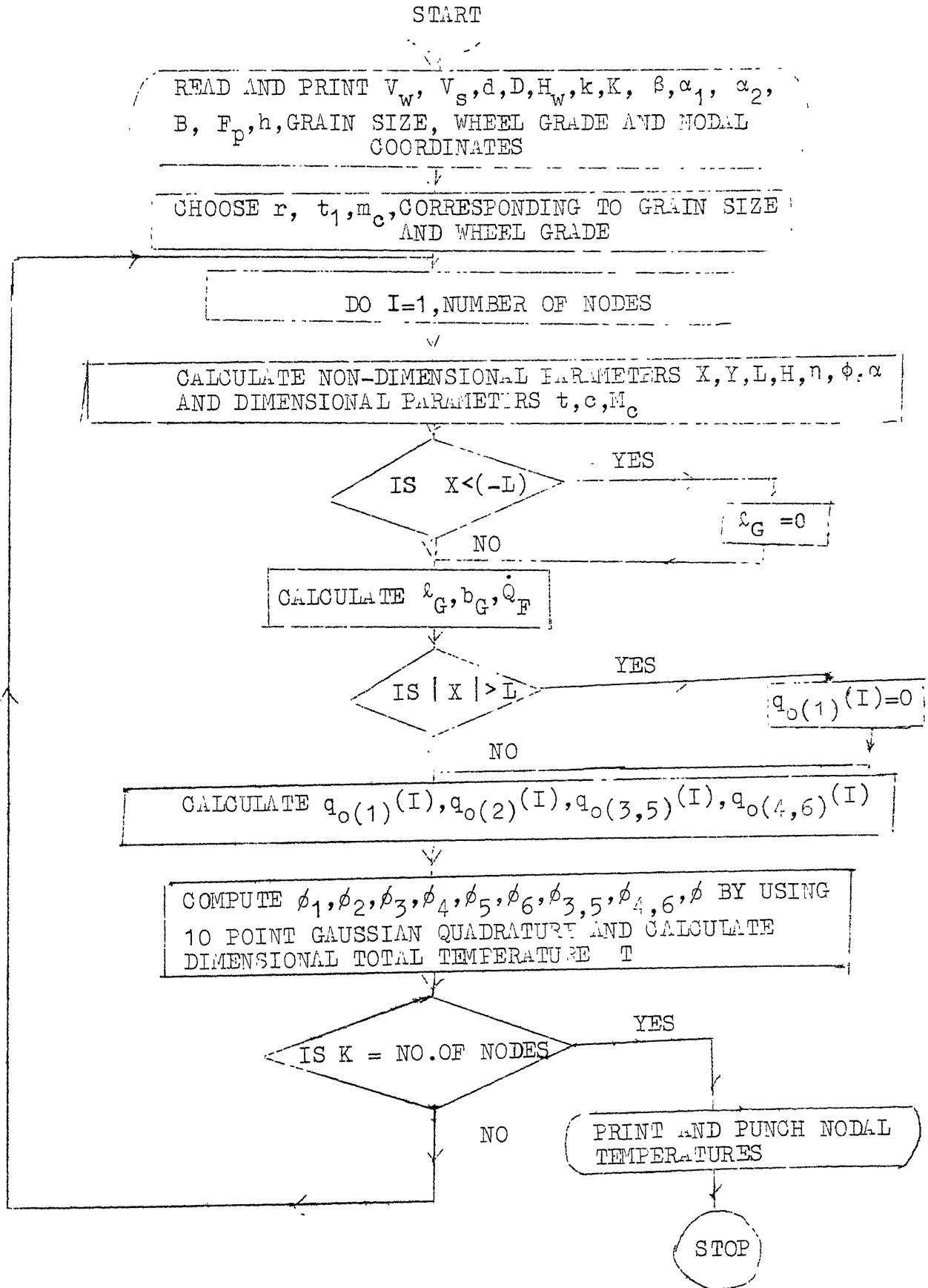

FIG.N.1: Computer flow chart for calculation of temperature distribution in the workpiece.

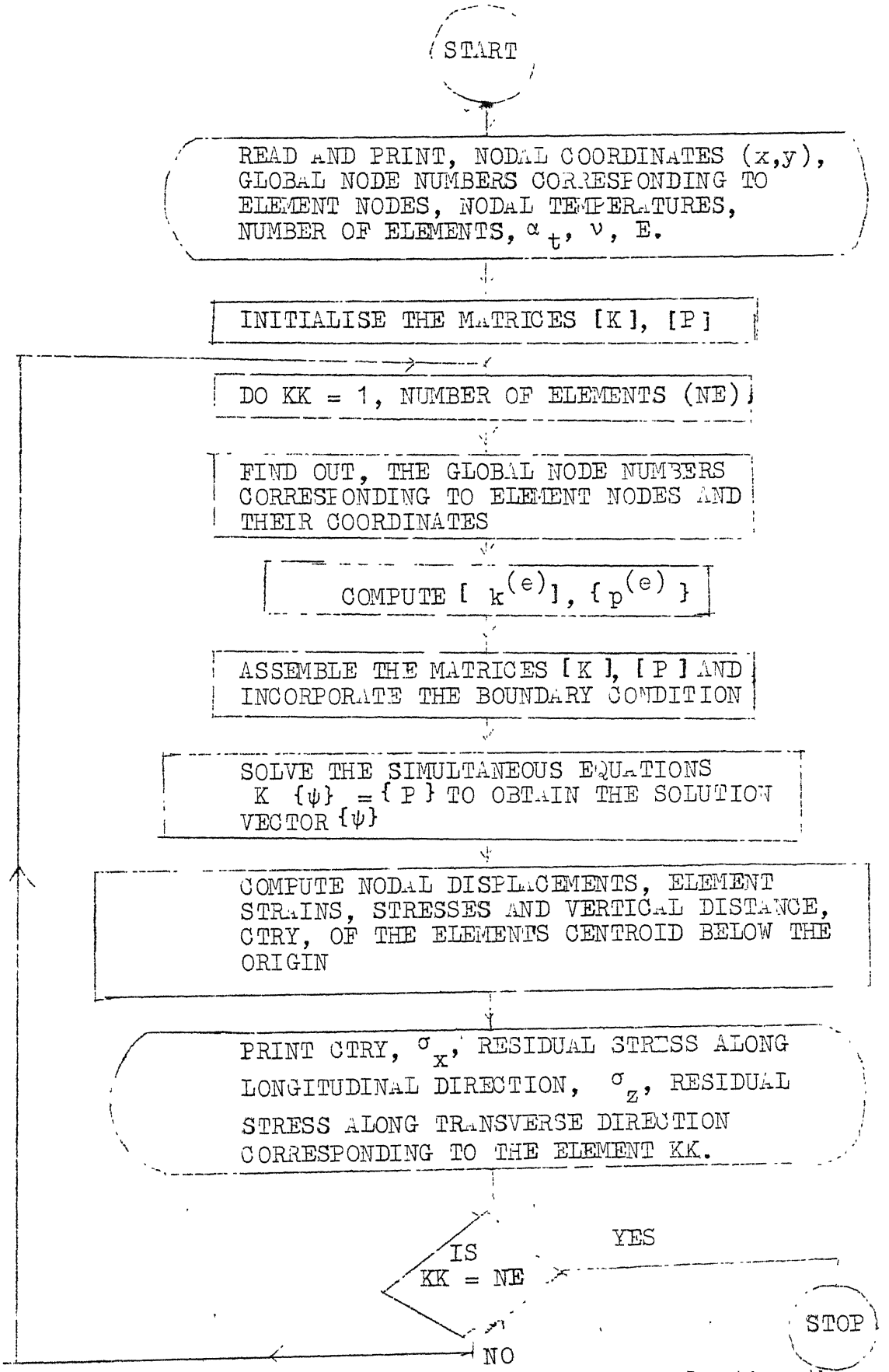

FIG.(N.2): Computer flow chart for evaluating the residual stress distribution by Finite element method.

CHAPTER 5

RESULTS AND DISCUSSION

As discussed earlier, the semi-infinite model has been used for calculating the steady state temperature distribution in the finite workpiece. Referring to Fig.(14), the steady state temperature distribution so obtained decays very fast with the depth below the surface. It becomes almost negligible at a depth approximately equal to 0.075 in. (≈ 0.2 mm). This is sufficiently small compared to the total depth of the workpiece to justify the simulation of the finite workpiece as the semi-infinite body.

A typical residual stress distribution in the workpiece obtained by using the finite element method is shown in Fig. (15). It indicates that the layers very close to the surface are under high tensile stress. The stresses vary from tensile to compressive and the magnitude of these stresses decrease with increasing depth below the surface. However, from the experimental results available in the literature (14-21) it can be said that the nature and distribution of the residual stresses may vary widely with the grinding conditions. Positive values indicate tensile stresses and negative values indicate compressive stresses. Investigators in the past (14-21) have reported two stress values, one along the longitudinal direction and another along the transverse direction. It was shown that

the stresses in other directions will have intermediate values that lie between the two stress values mentioned. Hence, the distribution of residual stresses in the longitudinal and transverse direction are only considered and are shown in Fig.(15). A typical residual stress distribution measured by Letner (21) is shown in Fig.(16) and a schematic residual stress distribution for the case of dominant thermal source as given by Solwell, etal. (19) is shown in Fig.(17). A good qualitative agreement can be seen between these figures. If the peak residual tensile stresses which occur at or near the surface reach the ultimate strength of the workpiece material, the thermal failure in the form of "grinding cracks" can occur. Thus, it can be concluded that the magnitude of the residual tensile stresses have to be minimised to avoid thermal failure of the workpiece.

The grinding parameters such as table speed, wheel speed, cooling ability of grinding fluid, depth of cut, hardness of workpiece material, grain size, wheel grade etc. have a direct influence on the residual stresses generated during grinding. Effect of these parameters on residual stress distribution had been studied in the past experimentally (21) to make the grinding operation more useful. This has been evaluated theoretically in the present work.

Referring to Fig.(18), the magnitude of peak residual tensile stresses decrease with increasing table speed. This

is because the fraction, α, of the total grinding energy entering the workpiece decreases (Table 1) as the table speed increases. Thus, the maximum temperature to which the workpiece is subjected decreases. On the other hand, at low table speeds, the reduction in the magnitude of residual stresses appear to be insignificant. At low table speeds the cooling property of the grinding fluid becomes so effective that it overcomes the effect of reduced table speeds. As a result of this, the temperature to which the workpiece is subjected is low. The obtained variation of residual stresses with table speed [Fig.18(a)] can be compared with the variation measured by Plusch (21) [Fig.18(b)] which shows good qualitative agreement.

Table 1 appears to indicate that the fraction, α, decreases with decreasing wheel speed. Thus the magnitude of residual stresses increases with increasing wheel speed. This is shown in Fig.(19). Field and Kahles (33) also found the residual stresses to increase with wheel speed [Fig.19(b)].

As the depth of cut is increased the fraction, α, increases. Consequently the maximum temperature at a point in the workpiece increases. Thus the peak residual tensile stresses increase with the increase in depth of cut. The effect of depth of cut on residual stress distribution as shown in Fig.(20) indicates this to be the case. One way of measuring the residual stress is by removing successive layers

from the work-piece surface and measuring the change in the curvature resulting from release of the stresses in each layer (12). Letner (12) has given the relationship between the magnitude of residual stresses and the corresponding curvature changes. In the experiments carried out by Kubsh(21), curvature change was found to increase with increasing depth of cut [Fig.(21)]. The results of Fig.(20) and Fig.(21) seem to match qualitatively.

It can be seen in Fig.(22) that the magnitude of peak residual tensile stress decreases with increasing convective coefficient of the grinding fluid. After reaching a certain value of convective coefficient this reduction in the magnitude of residual tensile stress is insignificant. This is because, the reduction in magnitude of peak residual tensile stress depends upon good convective property of the grinding fluid, while large variations in the cooling property [$h > 0.0005$ Btu/(in^2 sec °F)] has only a very small effect on the temperature rise and hence on residual stresses.

Malkin and Anderson (35) have shown that as the grain size (nominal grain diameter) is decreased, the number of active grains per unit area increases. Therefore, the strength of the single grain heat source must decrease with decreasing grain size (increasing mesh number) resulting in lower heat energy generation which affects the residual stress distribution. Results shown in Fig.(23) also indicate

that the residual stress values decrease with decreasing grain size (increasing mesh number). This aspect, however, needs further investigation.

CHAPTER 6

CONCLUSION

The theoretical model using the finite element technique for evaluating the residual stress distribution in the workpiece during grinding appears to yield results which agree qualitatively with the published experimental results. It is observed that the magnitude of the peak residual tensile stress can reach the ultimate strength of the workpiece resulting in thermal failure of the workpiece. The grinding conditions have significant effect on the residual stress distribution.

The peak residual tensile stress appears to decrease with increasing table speed, decrease with decreasing wheel speed and increase with increasing depth of cut. The convective property of the grinding fluid also effects the residual stress distribution significantly.

6.1 Future Research

In the present work a theoretical model has been presented and it needs quantitative verification with experimental results. A sensitive method for measuring the residual stresses needs to be developed so that the effect of various grinding parameters could be evaluated. Further the theoretical model has been considered for single pass plunge-cut grinding. It needs to be extended

further to include the effect of successive grinding passes. The work could also be extended to include the effect of grinding wheel characteristics such as wheel hardness, grain size etc.

REFERENCES

1. Tarasov, L.P. and Lundberg, C.O., "Nature and detection of grinding burn in steel", Trans. ASME, Vol.41, p. 893, 1949.

2. Outwater, J.O. and Shaw, M.C., "Surface temperatures in grinding", Trans. ASME, Vol.74, p.73, 1952.

3. Mckee, R.E. and Wulff, J., "The influence of the grinding process on the structure of hardened steel", Trans. ASME, Vol.47, p.21, 1957.

4. Mayer, J.E. and Shaw, M.C., "Grinding temperatures", Lubrication Engineering, Vol.13, p. 21,1957.

5. Sato, K., "Grinding temperatures", Bulletin of Japan Society of Grinding Engineers, Vol.1, p.31, 1961.

6. DesRuisseaux, N.R. and Zerkle, R.D., "Thermal analysis of the grinding process", Trans. ASME, J. Engineering for Industry, Vol.92B, p.428, 1970.

7. Malkin, S. and Anderson, R.B., "Thermal aspects in grinding, Part 1-Energy partition, Part 2-surface temperatures and workpiece burn", Trans. ASME, J. Engineering for Industry, Vol. 96B, p.1177, 1974.

8. Sauer, W.G.,"Thermal aspects of surface grinding", New developments in grinding, Proc. of the International Grinding Conference, p.391, 1972.

9. Sauer, W.G., "Thermal aspects of grinding", Ph.D. Thesis, Corneigie Mellon University, Pittsburg, Pa., 1971.

10. Carslaw, H.S. and Jaeger, J.C., "Conduction of heat in solids", Oxford University Press, London, 1947.

11. Jaeger, J.C., "Moving sources of heat and the temperature at sliding contacts", Proc. Royal Society of New Southwales, Vol.76, pt.3, p.203, 1942.

12. Letner, H.R., "Residual grinding stresses in hardened steel", Trans. ASME, Vol.77, p. 1089, 1955.

13. Letner, H.R., "Application of optical interference to to the study of residual surface stresses", Proc. Society for experimental Stress Analysis, Vol.10, p.23, 1953.

14. Letner, H.R., "Influence of grinding fluids upon residual stresses in hardened steels", Trans. ASME, Vol.79, p. 149, 1957.

15. Halverstadt, R.D., "Analysis of residual stresses in ground surfaces of high temperature alloys", Trans. ASME, Vol.30, p. 928, 1958.

16. Tarasov, L.P. and Lundberg, G.O., "Detection causes and prevention of injury to ground surfaces", Trans. ASME, Vol.36, p.389, 1946.

17. Glikman, L.A., Sanfirova, T.P. and Stepanov, V.A., "Origin of residual stresses in grinding nigh chromium stainless steels", J. Technical Physics, Vol.19, p.441, 1949.

18. Tarasov, L.P., Hyler, W.S. and Letner, H.R., "Effect of grinding conditions and resultant residual stresses on the fatigue strength of hardened steel", Proc. ASTM, vol.57, p.601, 1957.

19. Colwell, L.V., Simott, M.J. and Tobin, J.C., "The determination of residual stresses in hardened ground steel", Trans. ASME, vol.77, p.1099,1955.

20. Frisch, J. and Thomsen, E.G., "Residual grinding stresses in mild steel", Trans. ASME, Vol.73, p.337, 1951.

21. "Grinding Stresses - Cause, Effect and Control", collected papers, published by grinding wheel institute of America, Cleveland, Ohio, 1961.

22. Hann, R.S., "On the loss of surface integrity surface form due to thermo plastic stress in plunge grinding operation", Annals of CIRP, Vol.25, p. 203, 1976.

23. Nokano, Y., Uchida, and Ota, K., "Thermal deformation and profile errors of workpiece in surface grinding", Annals of CIRP, vol.25, p. 235, 1976.

24. Batra, J.L. "Grinding stresses in annealed low carbon steel using fractional design", Proc. 5th All India M.T.D.R. Conference, 1972.

25. Mishra, A., Rao, U.R.K. and Natarajan, R., "An analytical approach to the determination of residual stress in surface grinding", Proc. International Conference on Production Engineering, New Delhi, Vol.2, p.40, 1977.

26. Littmann, W.E., "Control of residual stresses in metal surfaces", Proc. CIRP International Conference on Manufacturing Technology, 1967.

27. Backer, W.R., etal., "The size effects in metal cutting", Trans. ASME,Vol.74, 1952.

28. Marshall, E.R., and Shaw, M.C.,"Forces in Dry Surface Grinding", Trans. ASME, Vol.74, 1952.

29. Reinchenbach, G.S., etal., "The role of chip thickness in grinding", Trans. ASME, Vol.74, 1952.

30. Nakayama, K. and Shaw, M.C., "An analytical study of the finish produced in surface grinding", Proc. Institution of Mechanical Engineers, Vol.182, Pt.3K, 1967.

31. Shaw, M.C., etal., "A New Theory of grinding", 4th Annual report of the Abrasive Grain Association Investigation, Carnegie-Mellon University, 1969.

32. Shaw, M.C. and Desalvo, G.J., "On the plastic flow beneath a blunt axisymmetric indenter", ASME, Paper No. 68-WA/prod., 12, 1969.

33. Field,M. and Kahles, J.F., "The surface integrity of machined and ground high strength steels", D.M.I.C. Report 210, Battle Memorial Institute, p. 54, 1964.

34. Shaw, M.C., "Fundamentals of grinding", New Developments in Grinding, Proc. International Grinding Conference, p. 220, 1972.

35. Malkin, S. and Anderson, R.B., "Active grains and dressing practices in grinding", New Developments in Grinding, Proc. International Grinding Conference, p.161, 1972.

36. Timeshenko, S.P. and Goodier, J.N., "Theory of Elasticity", Mc-Graw-Hill, London, 1970.

37. Desai, C.S. and Abel, J.F., "Introduction to the finite element method", Von Nostrand, Reinhold, New York, 1972.

38. Zienkiewicz, O.C., "The finite element method in engineering sciences", Mc-Graw-Hill, London, 1971.

39. Hastings, C., Jr., "Approximations for digital computers", Princeton, University Press, Princeton, New Jersey, 1955.

APPENDIX

The elements considered in the solution of equation(3.15) are subparametric triangular elements as shown below.

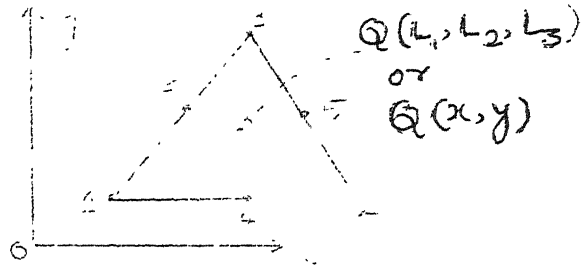

where 1,2,3 are the primary node numbers and 4,5,6 are the secondary node numbers. L_1, L_2, L_3 are the natural coordinates of a point, Q, in the element. The variation of thermo elastic displacement potential, ψ, within the element is taken as (38)

$$\overset{(e)}{\psi} = [N_1 \quad N_2 \quad N_3 \quad N_4 \quad N_5 \quad N_6] \begin{Bmatrix} \psi_1 \\ \psi_2 \\ \psi_3 \\ \psi_4 \\ \psi_5 \\ \psi_6 \end{Bmatrix} \qquad (A.1)$$

Here, the shape functions, [N] , are given by

$$N_1 = L_1(2L_1-1) \; ; \quad N_2 = L_2(2L_2-1); \quad N_3 = L_3(2L_3-1)$$

$$N_4 = 4L_1L_2 \quad ; \quad N_5 = 4L_2L_3 \quad ; \quad N_6 = 4L_1L_3 \qquad (A.2)$$

The Natural coordinates are related to the Cartesian coordinates (x,y) by the relationship (37)

$$\begin{bmatrix} L_1 \\ L_2 \\ L_3 \end{bmatrix} = \frac{1}{2A^{(e)}} \begin{bmatrix} (x_2y_3-x_3y_2) & (y_2-y_3) & (x_3-x_2) \\ (x_3y_1-x_1y_3) & (y_3-y_1) & (x_1-x_3) \\ (x_1y_2-x_2y_1) & (y_1-y_2) & (x_2-x_1) \end{bmatrix} \quad (A.3)$$

where (x_i, y_i) are the Cartesian coordinates of node i and the element area, $A^{(e)}$, is given by

$$A^{(e)} = \frac{1}{2} \begin{vmatrix} 1 & x_1 & y_1 \\ 1 & x_2 & y_2 \\ 1 & x_3 & y_3 \end{vmatrix} \quad (A.4)$$

The relations that are useful in simplifying the derivation of element stiffness matrix etc. are

$$a_{A1} = x_3-x_2 \qquad b_{A1} = y_2-y_3$$

$$a_{A2} = x_1-x_3 \qquad b_{A2} = y_3-y_1$$

$$a_{A3} = x_2-x_1 \qquad b_{A3} = y_1-y_2 \quad (A.5)$$

$$\int\int_{A^{(e)}} L_1^{p'} L_2^{q'} L_3^{r'} \, dA = \frac{p'!\, q'!\, r'!}{(p'+q'+r')!} 2A^{(e)} \quad (A.6)$$

and

$$\frac{\partial}{\partial x} = \sum_{i=1}^{3} \frac{\partial L_i}{\partial x} \frac{\partial}{\partial L_i} = \sum_{i=1}^{3} \frac{b_{Ai}}{2A^{(e)}} \frac{\partial}{\partial L_i}$$

$$\frac{\partial}{\partial y} = \sum_{i=1}^{3} \frac{\partial L_i}{\partial y} \frac{\partial}{\partial L_i} = \sum_{i=1}^{3} \frac{a_{Ai}}{2A^{(e)}} \frac{\partial}{\partial L_i} \quad (A.7)$$

The elements of the element stiffness matrix, $[k^{(e)}]$, and element load vector, $\{p^{(e)}\}$, are given by (38)

$$k_{ij}^{(e)} = \iint_{A^{(e)}} \left(\frac{\partial N_i}{\partial x} \frac{\partial N_j}{\partial x} + \frac{\partial N_i}{\partial y} \frac{\partial N_j}{\partial y} \right) dA \quad (3.18)$$

and $p_i^{(e)} = -\iint_{A^{(e)}} C N_i \, dA$ (3.19)

Using equations (A.2) through (A.7) and equations (3.18) and (3.19), the elements of element stiffness matrix and element load vector can be derived as

$$k_{11}^{(e)} = (b_{A1}^2 + a_{A1}^2)/4$$

$$k_{12}^{(e)} = -(b_{A1}b_{A2} + a_{A1}a_{A2})/12$$

$$k_{13}^{(e)} = -(b_{A1}b_{A3} + a_{A1}a_{A3})/12$$

$$k_{14}^{(e)} = (b_{A1}b_{A2} + a_{A1}a_{A2})/3$$

$$k_{15}^{(e)} = 0$$

$$k_{16}^{(e)} = (b_{A1}b_{A3} + a_{A1}a_{A3})/3$$

$$k_{22}^{(e)} = (b_{A2}^2 + a_{A2}^2)/4$$

$$k_{23}^{(e)} = -(b_{A2}b_{A3} + a_{A2}a_{A3})/12$$

$$k_{24}^{(e)} = (b_{A1}b_{A2} + a_{A1}a_{A2})/3$$

$$k_{25}^{(e)} = (b_{A2}b_{A3} + a_{A2}a_{A3})/3$$

$$k_{26}^{(e)} = 0$$

$$k_{33}^{(e)} = (b_{A3}^2 + a_{A3}^2)/4$$

$$k_{34}^{(e)} = 0$$

$$k_{35}^{(e)} = (b_{A2}b_{A3} + a_{A2}a_{A3})/3$$

$$k_{36}^{(e)} = (b_{A1}b_{A3} + a_{A1}a_{A3})/3$$

$$k_{44}^{(e)} = \frac{2}{3}(b_{A1}^2 + b_{A2}^2 + b_{A1}b_{A2} + a_{A1}^2 + a_{A2}^2 + a_{A1}a_{A2})$$

$$k_{45}^{(e)} = \frac{1}{3}(b_{A2}^2 + b_{A1}b_{A2} + b_{A2}b_{A3} + 2b_{A1}b_{A3} + a_{A2}^2 + a_{A1}a_{A2} + a_{A2}a_{A3} + 2a_{A1}a_{A3})$$

$$k_{46}^{(e)} = \frac{1}{3}(b_{A1}^2 + b_{A1}b_{A2} + 2b_{A2}b_{A3} + b_{A1}b_{A3} + a_{A1}^2 + a_{A1}a_{A2} + 2a_{A2}a_{A3} + a_{A1}a_{A3})$$

$$k_{55}^{(e)} = \frac{2}{3}(b_{A2}^2 + b_{A3}^2 + b_{A2}b_{A3} + a_{A2}^2 + a_{A3}^2 + a_{A2}a_{A3})$$

$$k_{56}^{(e)} = \frac{1}{3}(b_{A3}^2 + 2b_{A1}b_{A2} + b_{A2}b_{A3} + b_{A1}b_{A3} + a_{A3}^2 + 2a_{A1}a_{A2} + a_{A2}a_{A3} + a_{A1}a_{A3})$$

$$k_{66}^{(e)} = \frac{2}{3}(b_{A1}^2 + b_{A3}^2 + b_{A1}b_{A3} + a_{A1}^2 + a_{A3}^2 + a_{A1}a_{A3}) \qquad (A.8)$$

Here $[k^{(e)}]$ is a symmetric matrix, i.e. $k_{ij} = k_{ji}$.

and

$$p_i^{(e)} = -\frac{C\,A^{(e)}}{3}\begin{Bmatrix} 0 \\ 0 \\ 0 \\ 1 \\ 1 \\ 1 \end{Bmatrix} \qquad (A.9)$$

Partial derivatives of the shape functions to be used in equations (3.23) are

$$\frac{\partial N_1}{\partial x} = \frac{1}{A^{(e)}}(2b_{A1}L_1 - \frac{b_{A1}}{2}); \quad \frac{\partial N_1}{\partial y} = \frac{1}{A^{(e)}}(2a_{A1}L_1 - \frac{a_{A1}}{2})$$

$$\frac{\partial N_2}{\partial x} = \frac{1}{A^{(e)}}(2b_{A2}L_2 - \frac{b_{A2}}{2}); \quad \frac{\partial N_2}{\partial y} = \frac{1}{A^{(e)}}(2a_{A2}L_2 - \frac{a_{A2}}{2})$$

$$\frac{\partial N_3}{\partial x} = \frac{1}{A^{(e)}}\left(2b_{A3}L_3 - \frac{b_{A3}}{2}\right) \; ; \quad \frac{\partial N_3}{\partial y} = \frac{1}{A^{(e)}}\left(2a_{A3}L_3 - \frac{a_{A3}}{2}\right)$$

$$\frac{\partial N_4}{\partial x} = \frac{1}{A^{(e)}}\left(2b_{A1}L_2 + 2b_{A2}L_1\right); \quad \frac{\partial N_4}{\partial y} = \frac{1}{A^{(e)}}\left(2a_{A1}L_2 + 2a_{A2}L_1\right)$$

$$\frac{\partial N_5}{\partial x} = \frac{1}{A^{(e)}}\left(2b_{A2}L_3 + 2b_{A3}L_2\right); \quad \frac{\partial N_5}{\partial y} = \frac{1}{A^{(e)}}\left(2a_{A2}L_3 + 2a_{A3}L_2\right)$$

$$\frac{\partial N_6}{\partial x} = \frac{1}{A^{(e)}}\left(2b_{A1}L_3 + 2b_{A3}L_1\right); \quad \frac{\partial N_6}{\partial y} = \frac{1}{A^{(e)}}\left(2a_{A1}L_3 + 2a_{A3}L_1\right) \qquad (A.10)$$

The matrix of the derivatives of shape functions to be used in equation (3.24) are

$$\begin{bmatrix} \frac{\partial^2 N}{\partial x^2} \\ \frac{\partial^2 N}{\partial y^2} \\ \frac{\partial^2 N}{\partial x\, y} \end{bmatrix} = \frac{1}{A^{(e)2}} \begin{bmatrix} b_{A1}^2 & b_{A2}^2 & b_{A3}^2 & 2b_{A1}b_{A2} & 2b_{A2}b_{A3} & 2b_{A1}b_{A3} \\ a_{A1}^2 & a_{A2}^2 & a_{A3}^2 & 2a_{A1}a_{A2} & 2a_{A2}a_{A3} & 2a_{A1}a_{A3} \\ 2a_{A1}b_{A1} & 2a_{A2}b_{A2} & 2a_{A3}b_{A3} & 2(a_{A1}b_{A2} + a_{A2}b_{A1}) & 2(a_{A2}b_{A3} + a_{A3}b_{A2}) & 2(a_{A1}b_{A3} + a_{A3}b_{A1}) \end{bmatrix}$$

where $[N] = [\, N_1 \;\; N_2 \;\; N_3 \;\; N_4 \;\; N_5 \;\; N_6 \,]$.

Table 1(a): Input data for calculating temperature distribution. After Sauer (9). (Workpiece material AISI 1018 Cr steel)

Set No.	V_s ips	V_w ips	d in.	F_p lbf	h $\frac{Btu}{in^2\ sec\ F^o}$	α_1	α_2	α
1	770	6.0	0.00105	13.4	0.0000	0.6912	0.0000	0.6912
2	770	7.5	0.0011	16.4	0.0000	0.4393	0.1186	0.5579
3	770	7.95	0.00056	10.2	0.0010	0.7298	0.0000	0.7298
4	750	9.5	0.0011	29.9	0.0000	0.5143	0.0086	0.5229
5	770	10.9	0.0010	30,5	0.0000	0.2172	0.0974	0.3146
6	750	6.6	0.0011	13.8	0.0000	0.1420	0.1366	0.2786
7	750	9.5	0.00102	21.3	0.0057	0.4270	0.0499	0.4769
8	750	12.1	0.00099	26.5	0.0017	0.3389	0.0374	0.3763
9	750	9.2	0.00098	23.8	0.0005	0.3387	0.0140	0.3527
10	750	9.2	0.00102	22.7	0.0007	0.4283	0.0000	0.4283
11	750	9.6	0.00095	12.5	0.0001	0.6589	0.0000	0.6589
12	1360	9.8	0.00096	7.0	0.0001	0.6200	0.0000	0.6200
13	750	0.0270	0.0305	5.9	0.0053	0.1350	0.0395	0.1745
14	750	0.0275	0.0155	2.59	0.0028	0.0073	0.0878	0.0951
15	750	0.0570	0.0310	6.25	0.0025	0.0642	0.0427	0.1069
16	750	9.5	0.00102	21.3	0.0057	0.4270	0.0499	0.4769

Table 1(b): Results of the present work.

Set No.	1	2	3	4	5	6	7	8	9	10	11	12	13	14	15	16
Max. T_k^o	731	606	698	699	511	371	625	623	575	641	673	648	277	283	277	598
Peak σ_x $10^6 N/m^2$	345	242	304	248	152	96.5	214	159	186	221	228	214	20.7	6.9	21.4	193
Peak σ_z $10^6 N/m^2$	298	180	200	186	110	69	159	124	138	166	166	159	17.3	6.2	17.3	145
Grain size	60	60	60	60	60	60	60	60	60	60	60	60	60	60	60	80

Table 1(c): Average properties of the workpiece material. After Sauer (9).

Property	Symbol	Value	
Thermal diffusivity	k	0.01931	in^2/sec
Hardness	H_w	80000	lbf
Thermal conductivity	K	0.000674	Btu/(in sec F^o)
Decay coefficient	β	27.73	1/in.
Elastic modulus	E	$30x10^6$	psi
Thermal coefficient of linear expansion	α_t	$0.6435x10^{-5}$	$1/F^o$
Poisson ratio	ν	0.30	

CENTRAL LIBRARY
Acc. No. 54018

Table 2: The constants in equation (2.5). After Sauer (9).

Wheel type	t_1	m_c
24H	0.000007	2.0
60H	0.0000147	3.0
80H	0.000029	6.0

Table 3: Ratio, r, of undeformed chip width to chip thickness. After Sauer (9).

Grain size	Ratio r
36	18
46	15
60	12.5
80	10
120	7.6

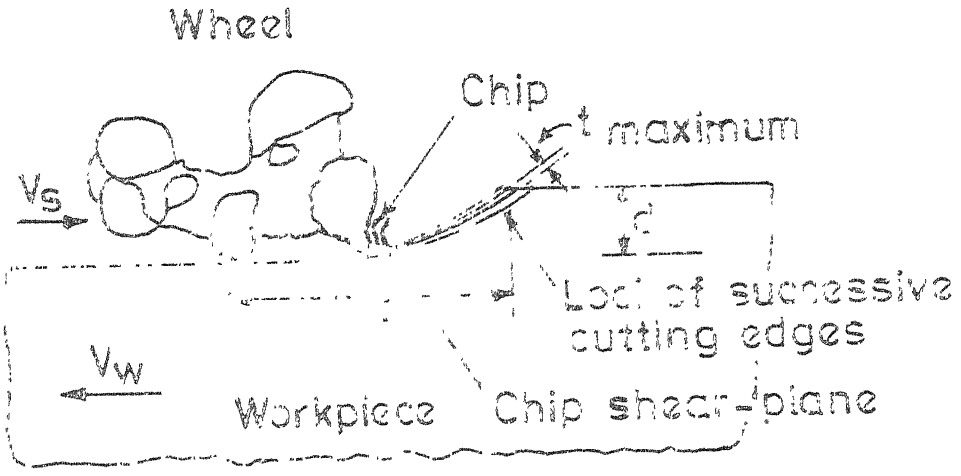

FIG. 1 CHIP FORMATION PROCESS [AFTER DES RUISSAUX et al (6)]

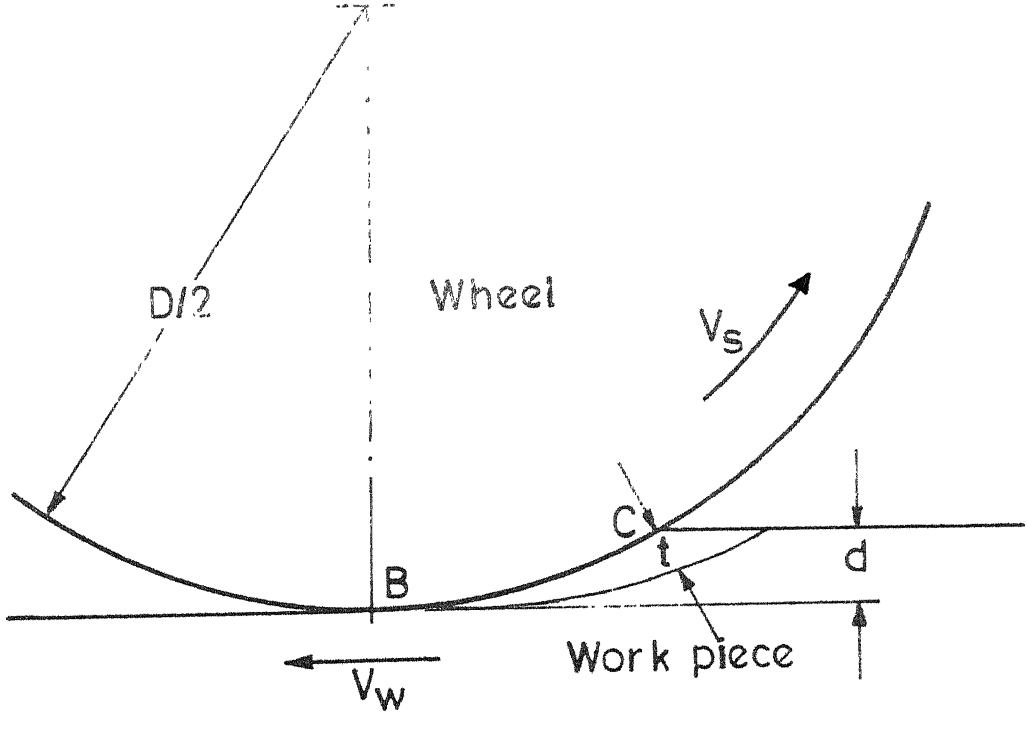

FIG. 2 INTERFERENCE ZONE

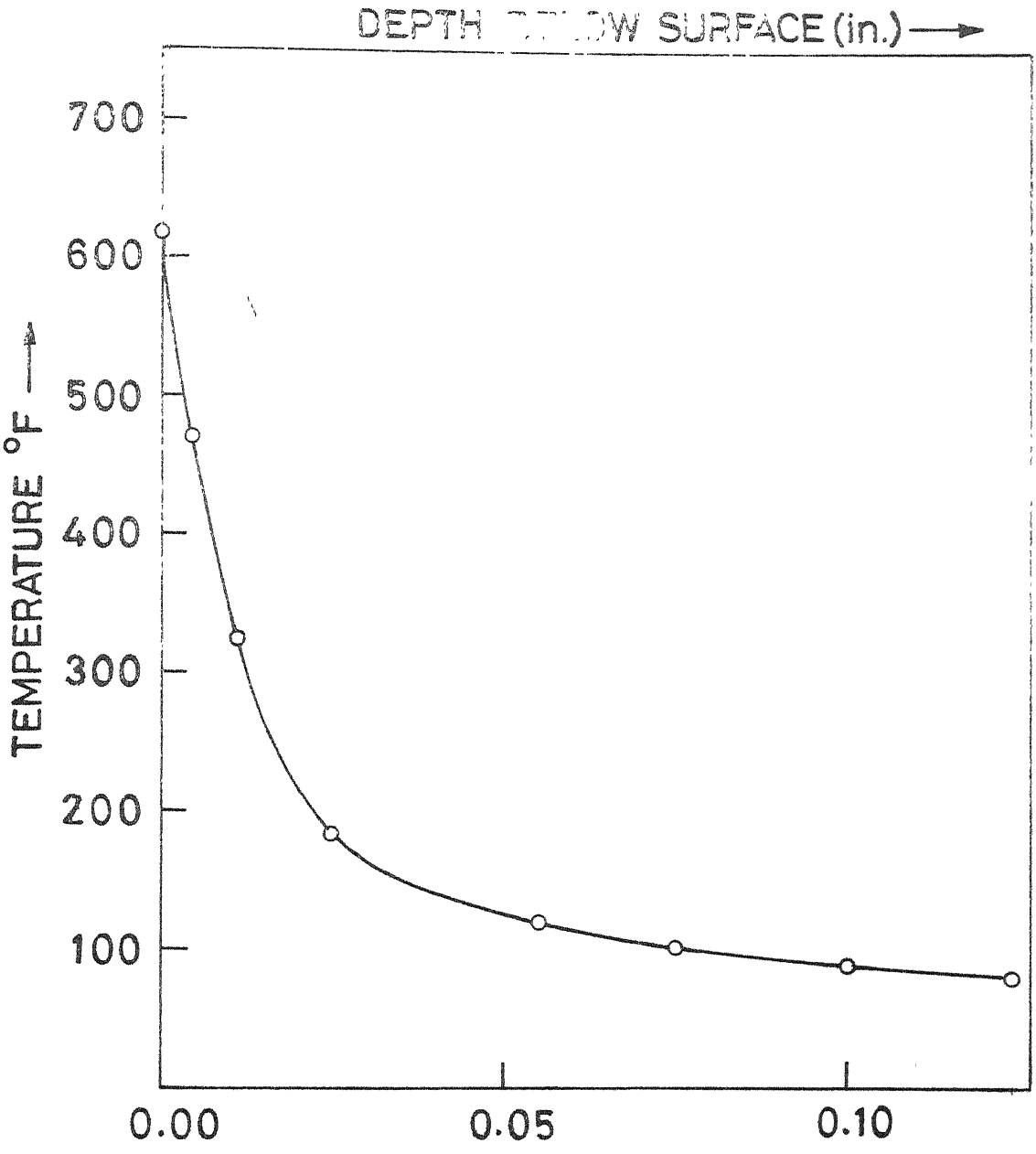

FIG. 3 A TYPICAL TEMPERATURE DISTRIBUTION IN SURFACE GRINDING. AFTER SAUER (9).

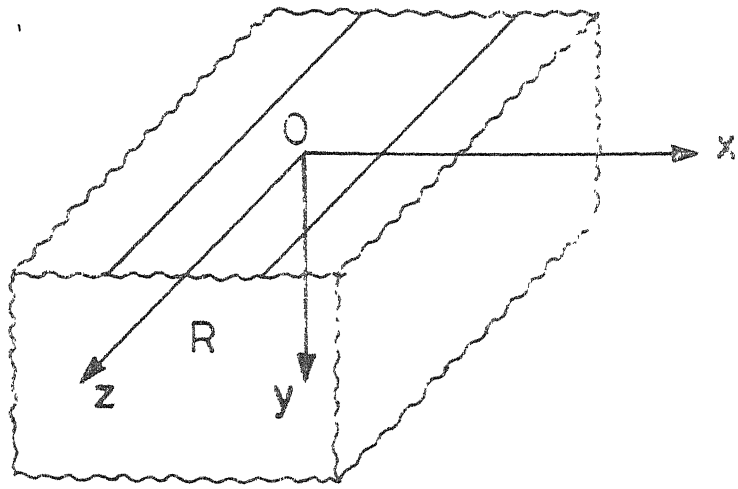

FIG. 5 MATHEMATICAL MODEL OF WORK PIECE IN SURFACE GRINDING.

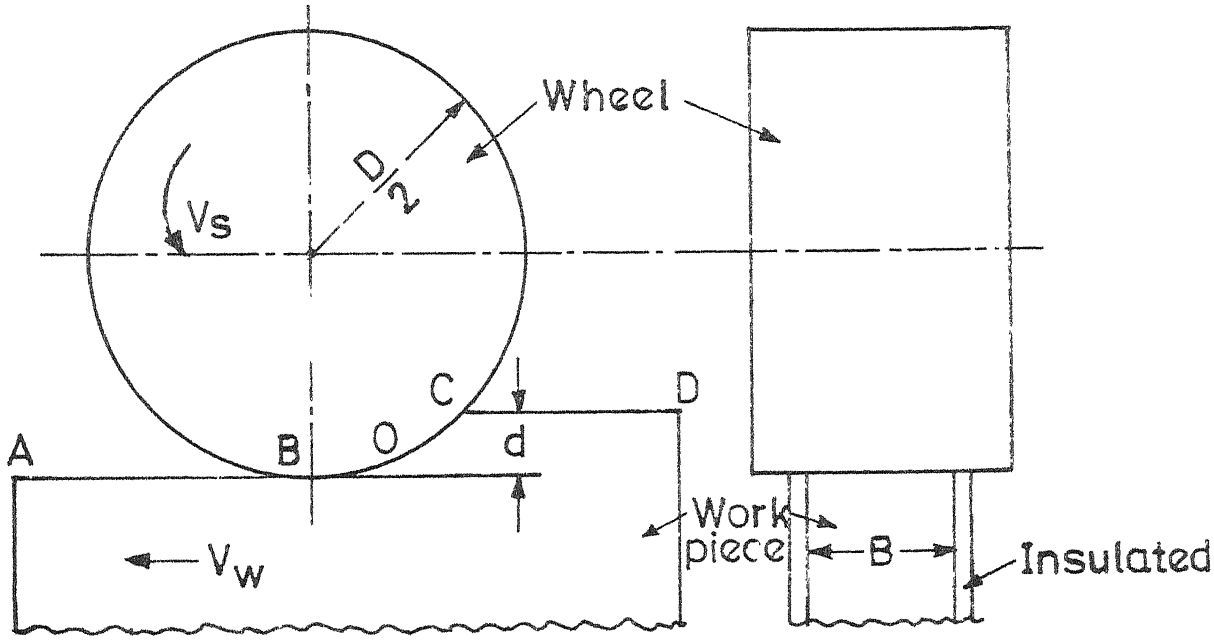

FIG. 6 PLUNGE-CUT SURFACE GRINDING

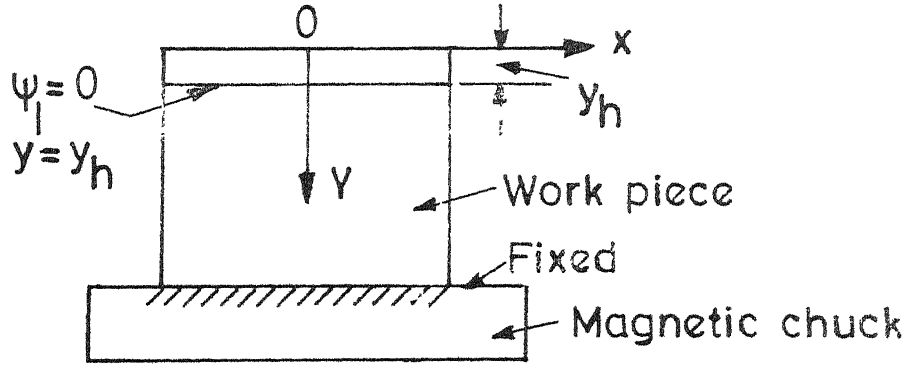

FIG. 7 BOUNDARY CONDITION

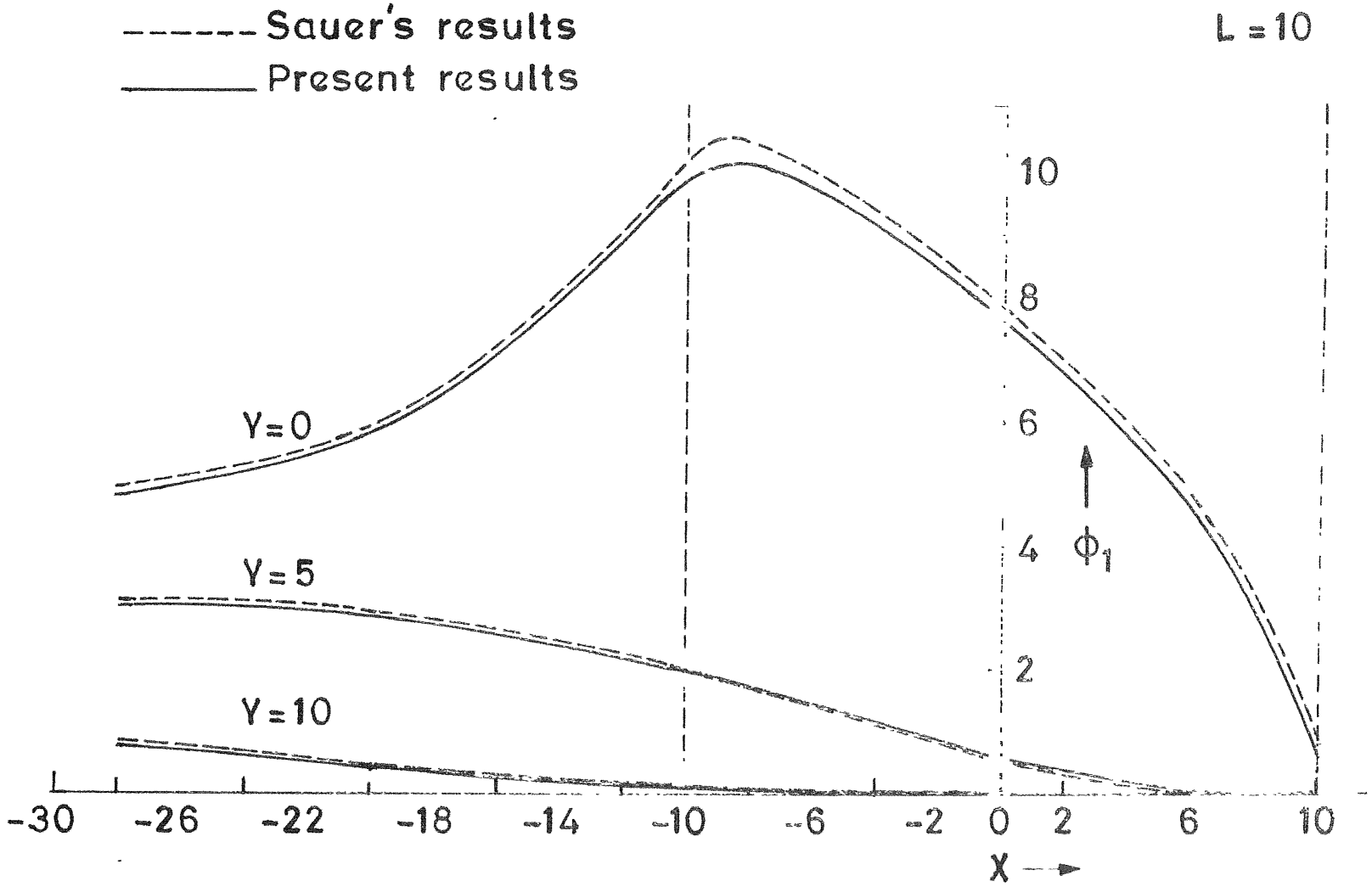

FIG. 8 VARIATION OF NON-DIMENSIONAL TEMPERATURE (ϕ_1) FOR CONSTANT SURFACE HEAT SOURCE WITHOUT CONVECTIVE COOLING.

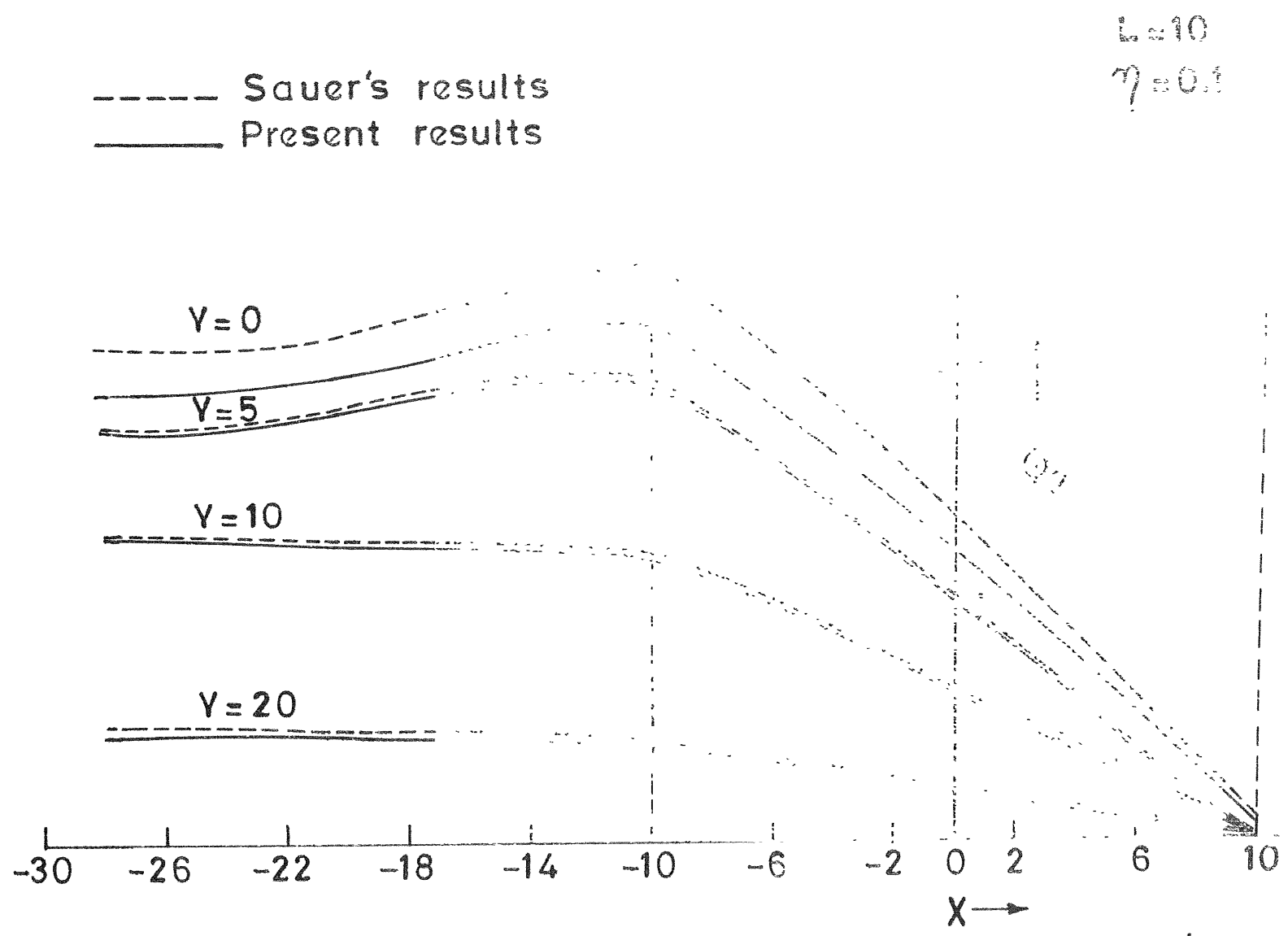

FIG.9 VARIATION OF NON-DIMENSIONAL TEMPERATURE (ϕ_2) WITHOUT CONVECTIVE COOLING FOR CONSTANT VOLUME HEAT SOURCE.

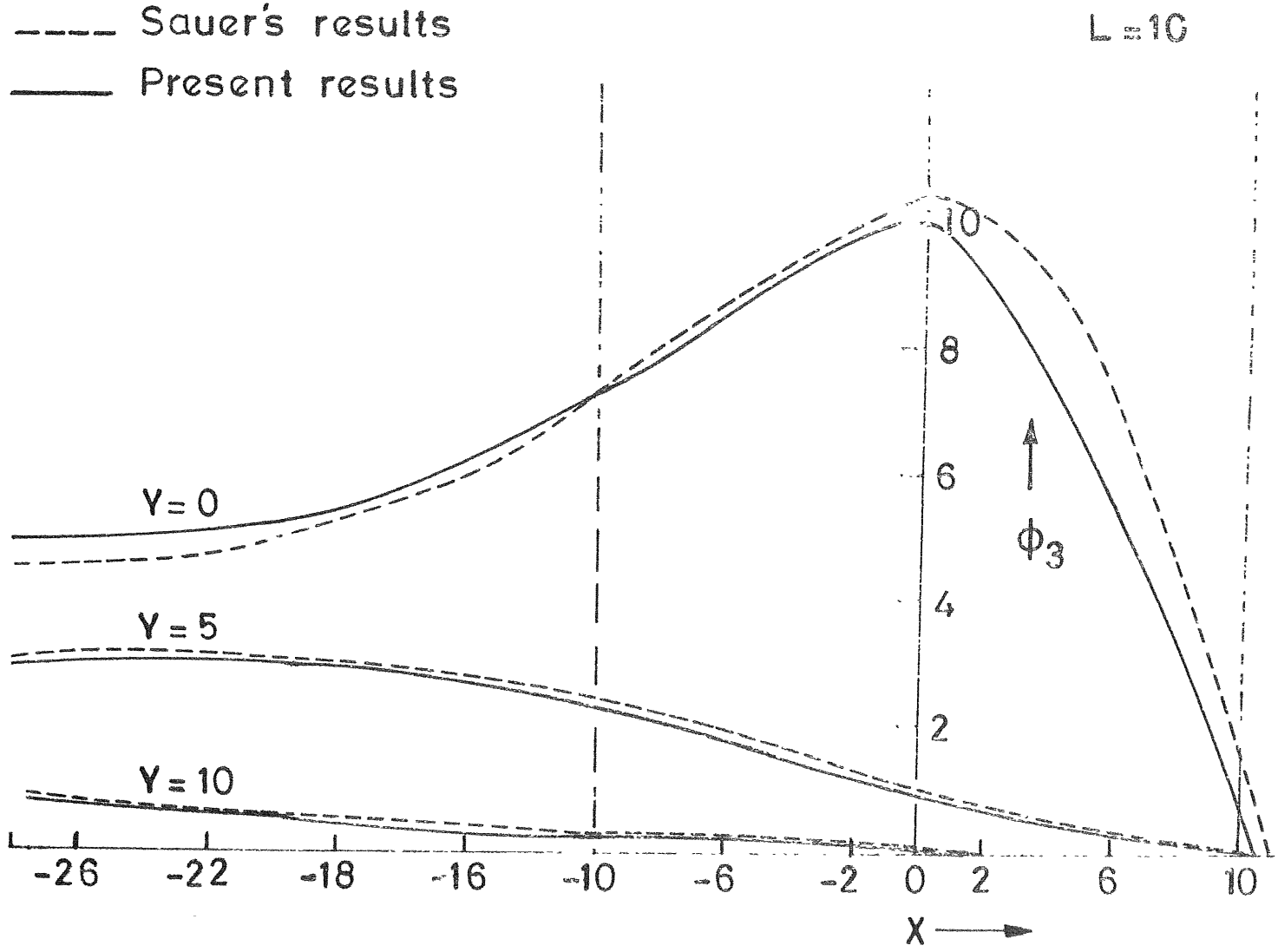

FIG.10 VARIATION OF NON-DIMENSIONAL TEMPERATURE (ϕ_3) WITHOUT CONVECTIVE COOLING FOR LINEARLY VARYING SURFACE HEAT SOURCE.

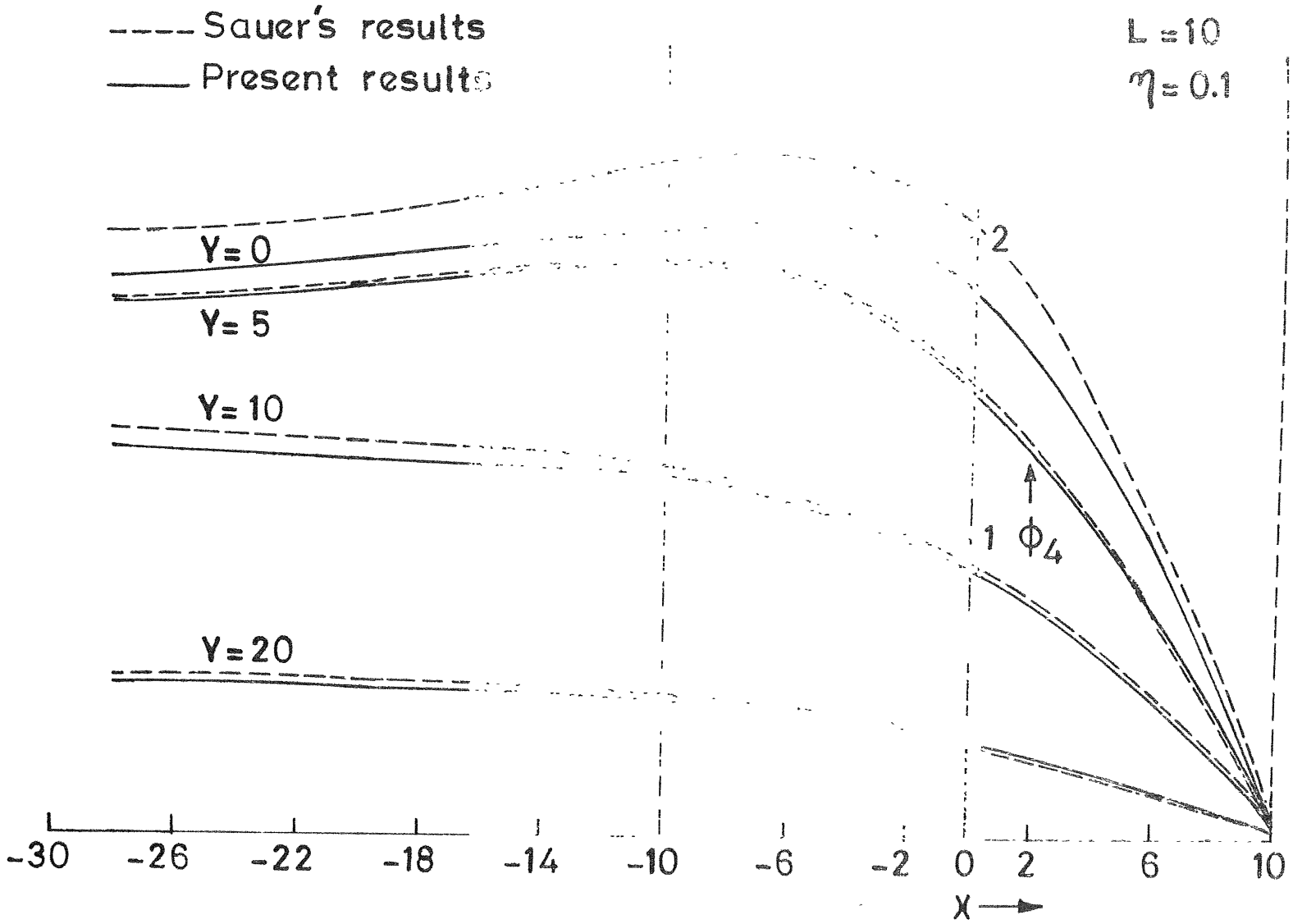

FIG.11 VARIATION OF NON-DIMENSIONAL TEMPERATURE (ϕ_4) FOR LINEARLY VARYING VOLUME HEAT SOURCE WITHOUT CONVECTIVE COOLING.

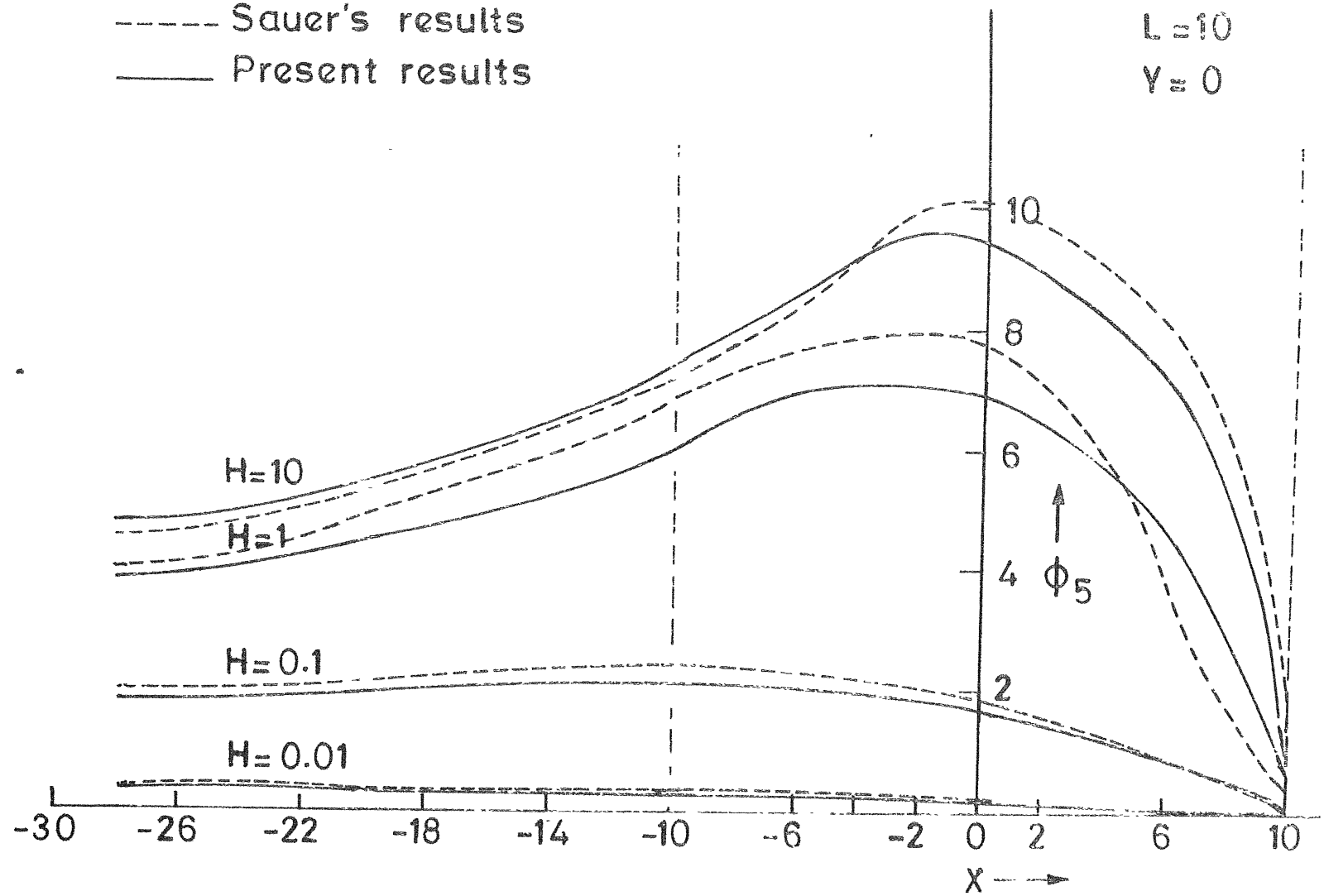

FIG.12 VARIATION OF NON-DIMENSIONAL TEMPERATURE (ϕ_5) WITH CONVECTIVE COOLING FOR LINEARLY VARYING SURFACE HEAT SOURCE.

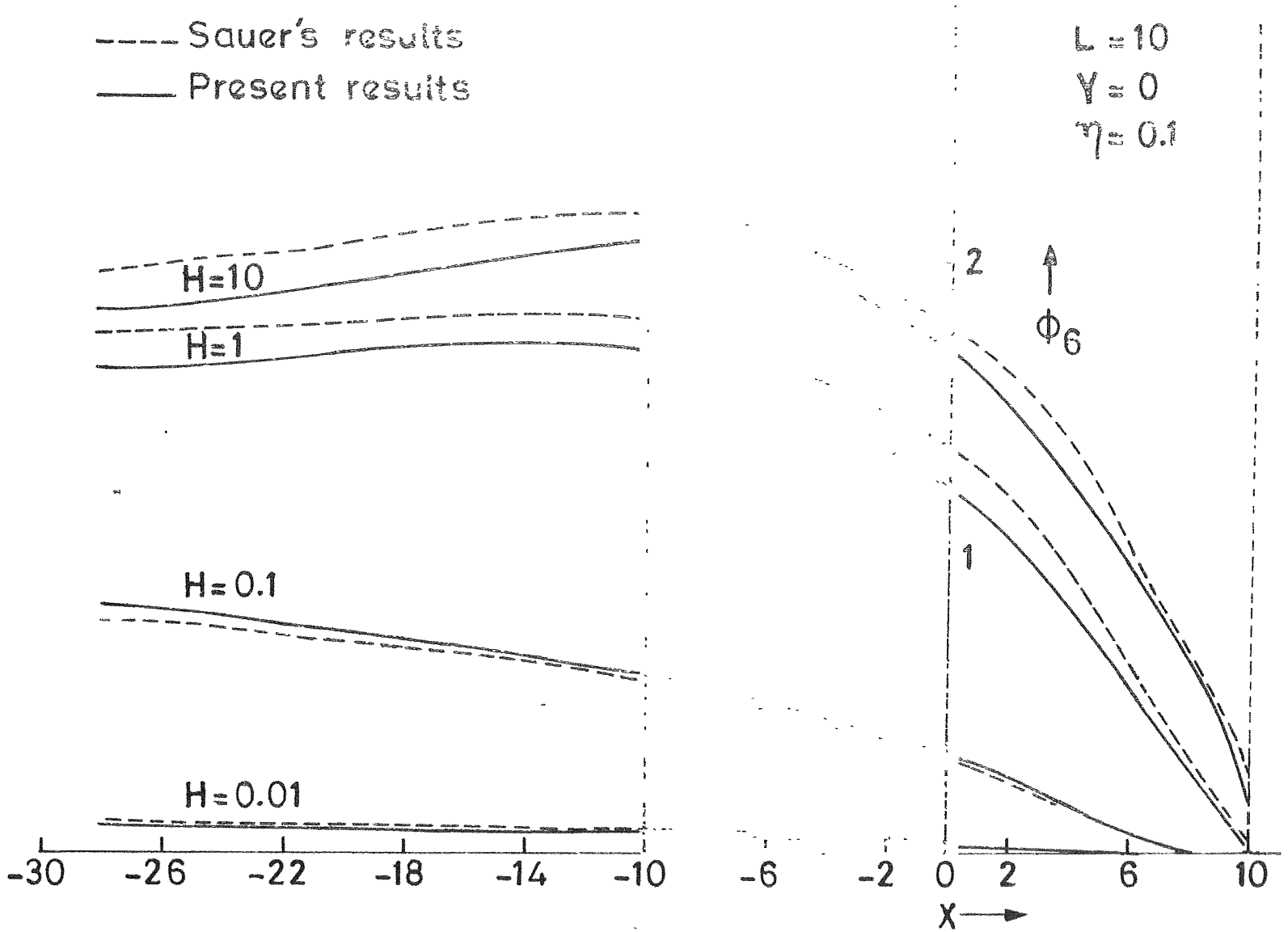

FIG.13 VARIATION OF NON-DIMENSIONAL TEMPERATURE (ϕ_6) WITH CONVECTIVE COOLING FOR LINEARLY VARYING VOLUME HEAT SURFACE.

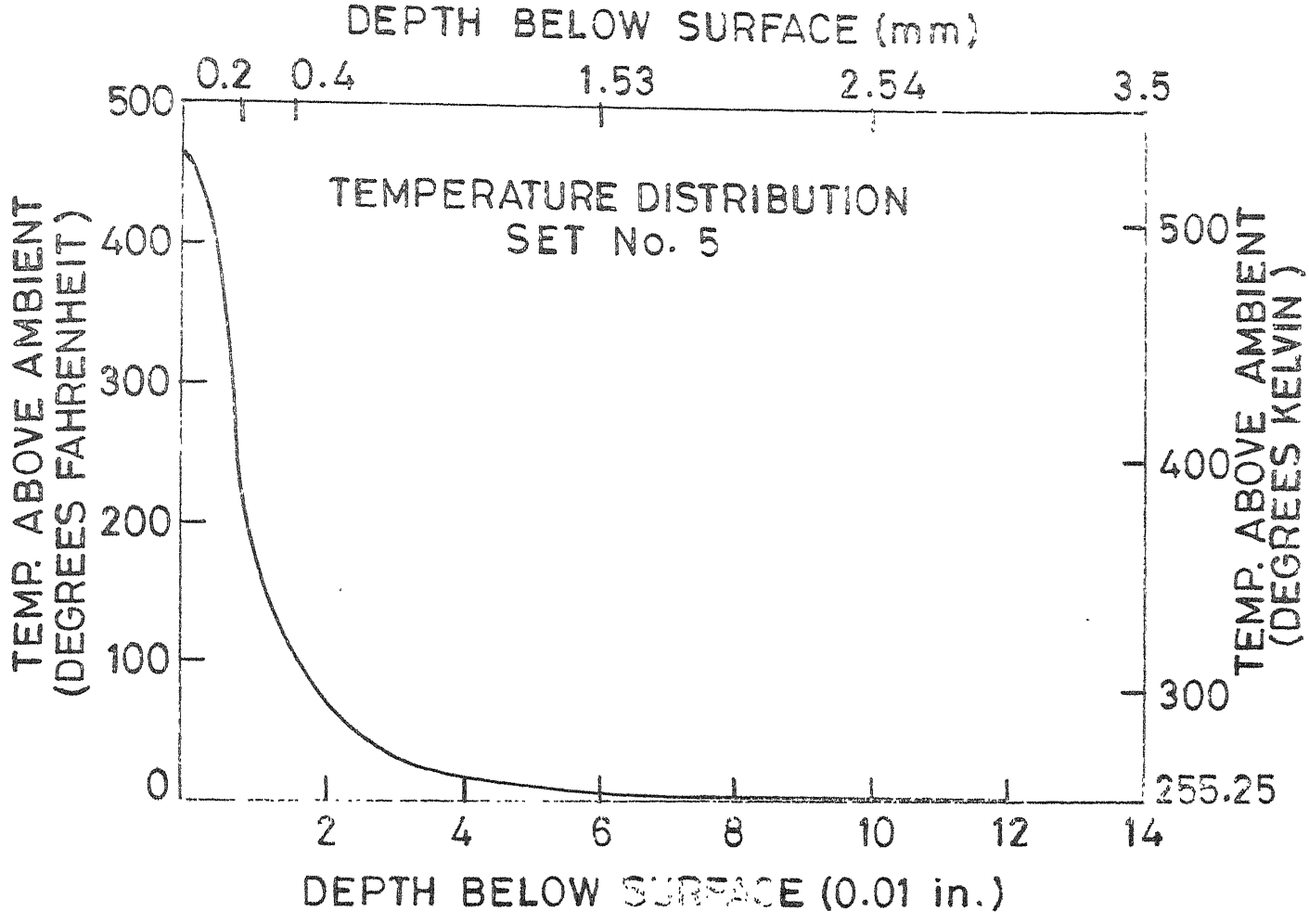

FIG. 14 TEMPERATURE DISTRIBUTION IN THE WORK-PIECE.

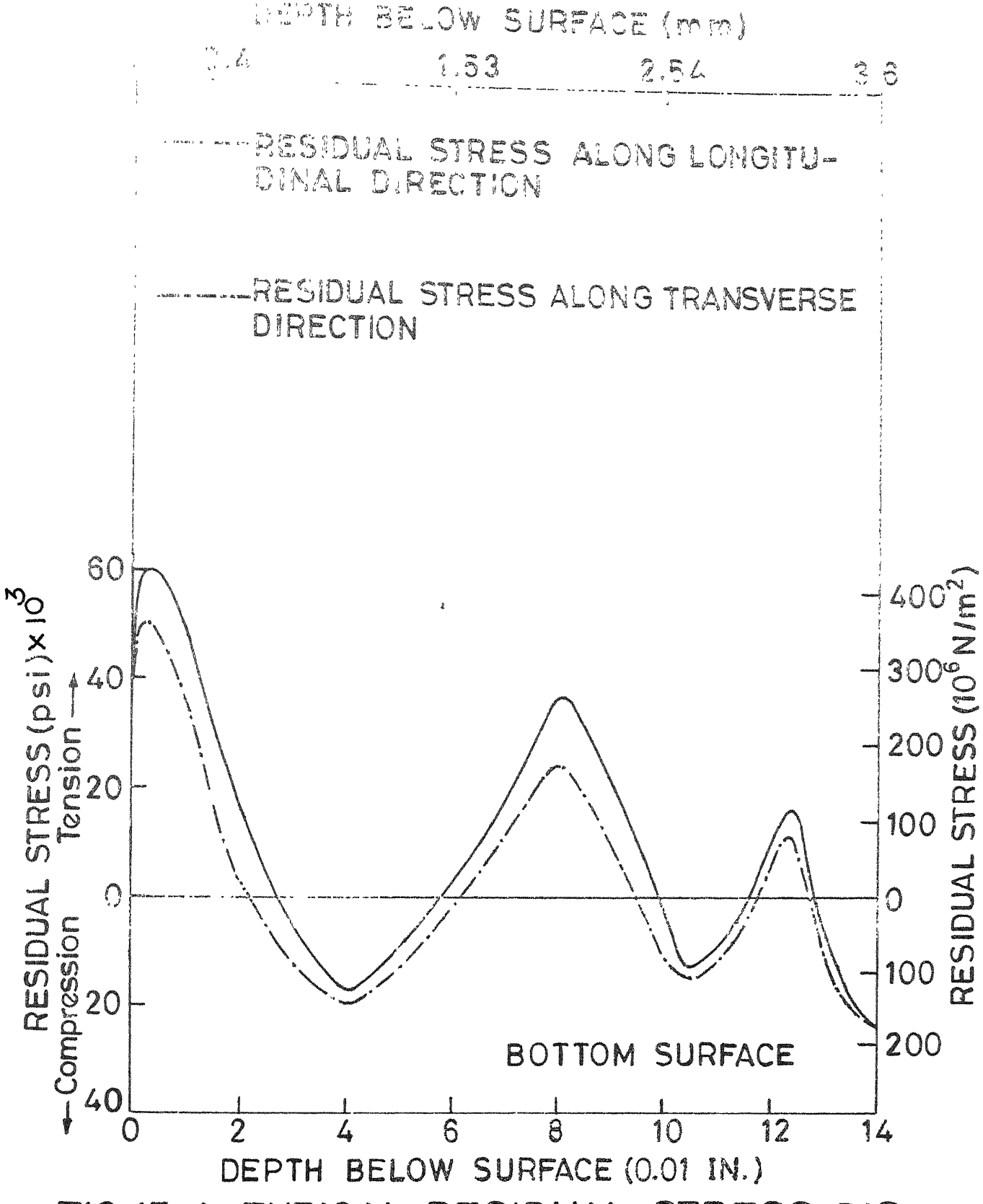

FIG.15 A TYPICAL RESIDUAL STRESS DISTRIBUTION FOR GRINDING CONDITIONS SET No.1, TABLE (1)

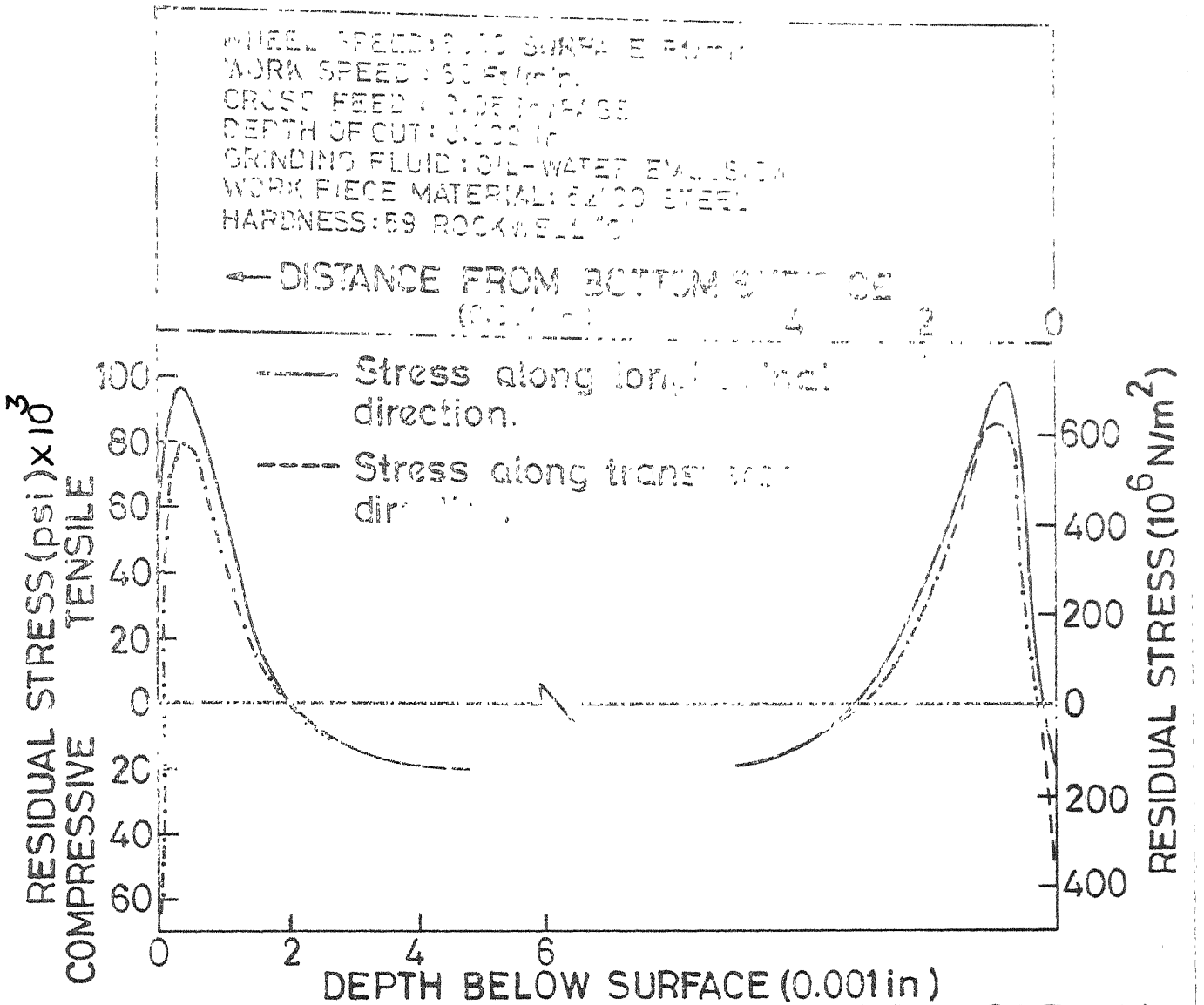

FIG.16 A TYPICAL RESIDUAL STRESS DISTRIBUTION. AFTER LETNER (12)

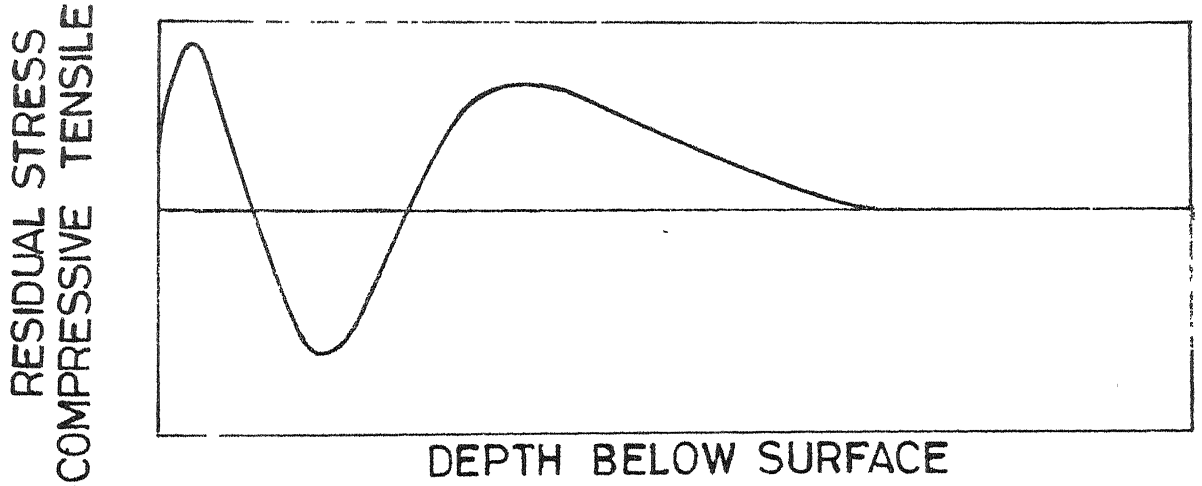

FIG.17 SCHEMATIC RESIDUAL STRESS DISTRIBUTION CURVE FOR THE CASE OF THERMAL SOURCE. AFTER COLWELL et al (19)

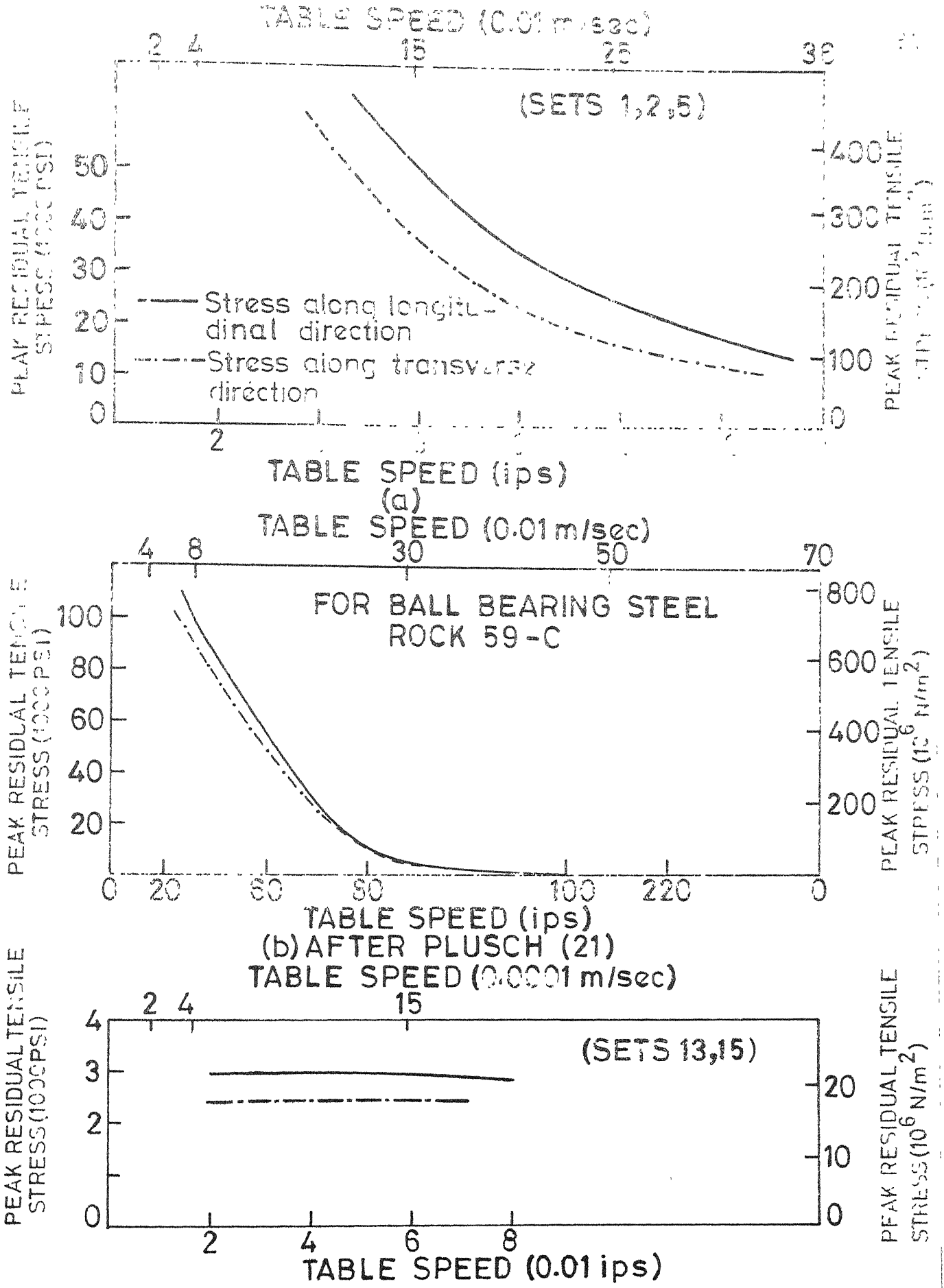

FIG.18 EFFECT OF TABLE SPEED ON RESIDUAL STRESS DISTRIBUTION

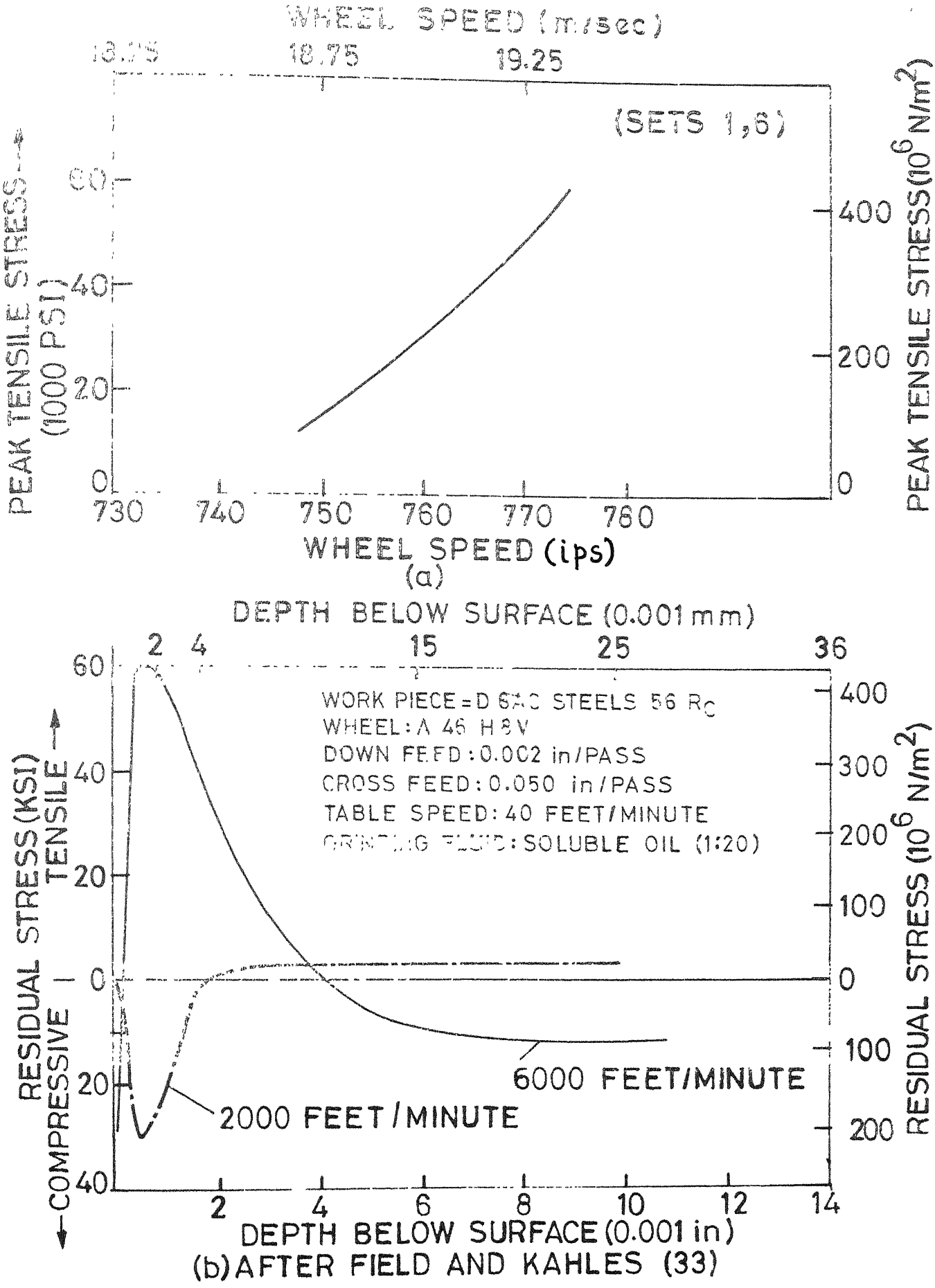

FIG.19 EFFECT OF WHEEL SPEED ON RESIDUAL STRESS DISTRIBUTION.

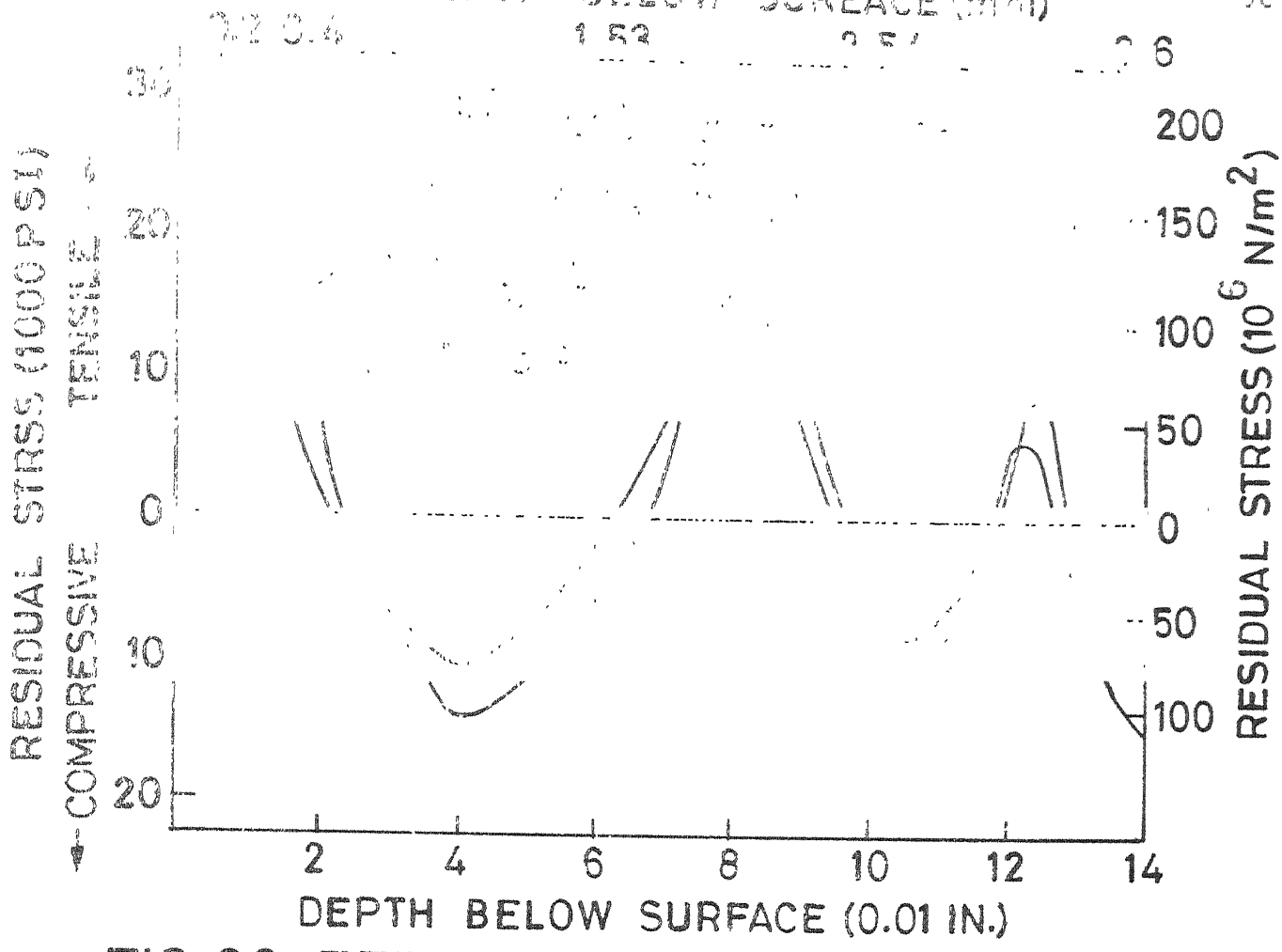

FIG. 20 EFFECT OF DEPTH OF CUT ON RESIDUAL STRESS DISTRIBUTION

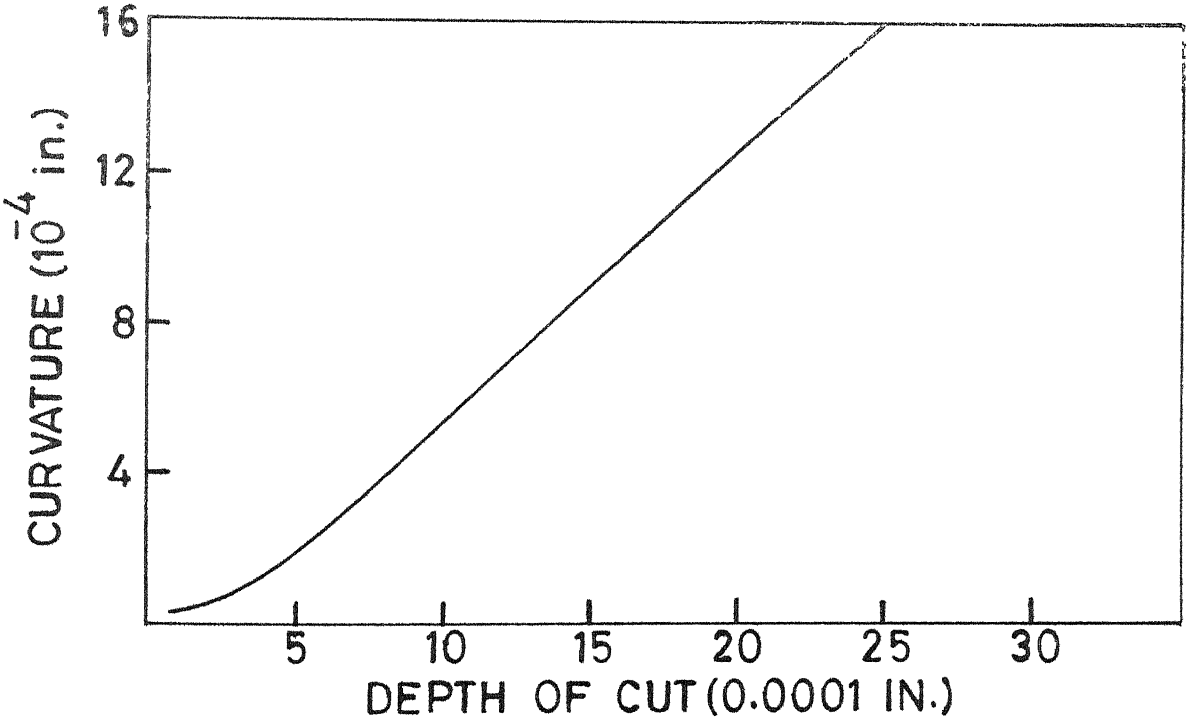

FIG. 21 EFFECT OF DEPTH OF CUT ON CURVATURE CHANGE. AFTER KUBSH (21)

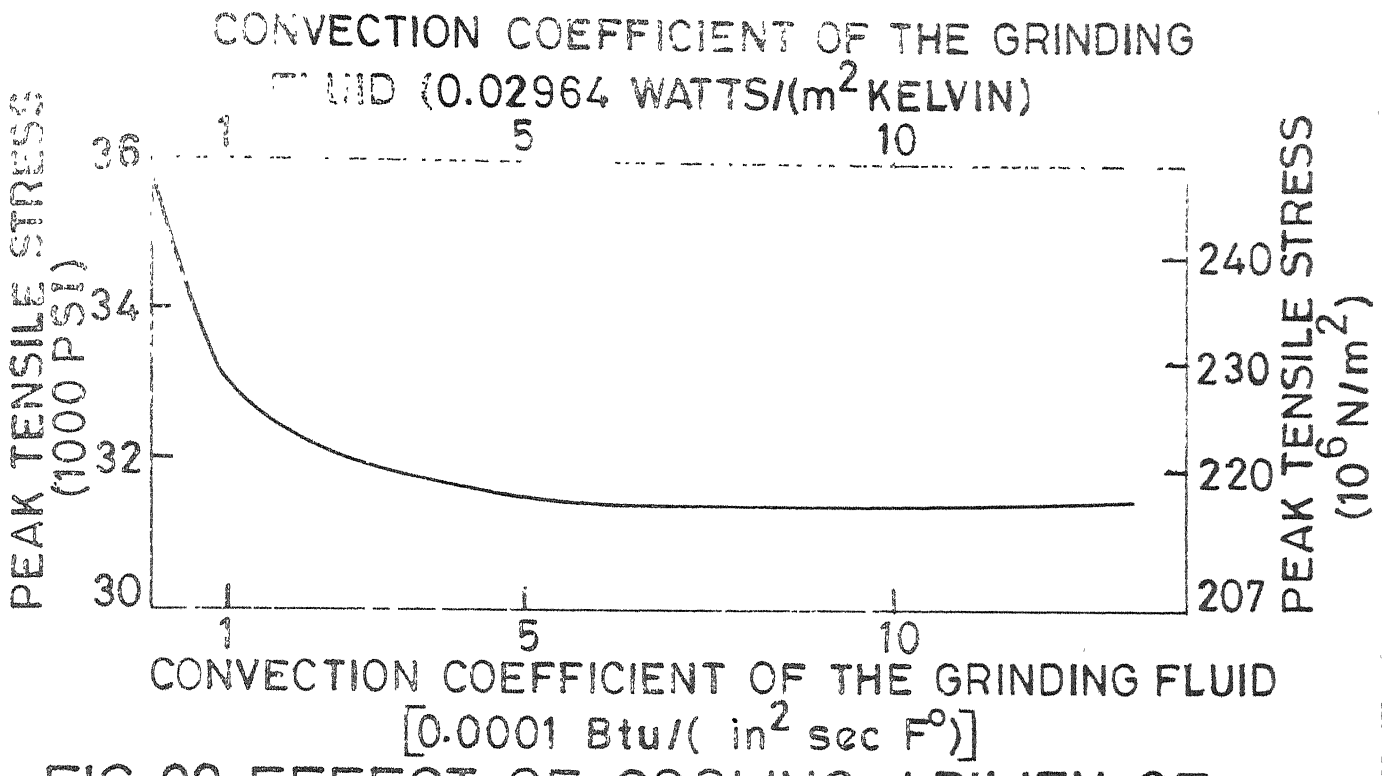

FIG. 22 EFFECT OF COOLING ABILITY OF GRINDING FLUID ON RESIDUAL STRESS DISTRIBUTION FOR SETS 4,10,11.

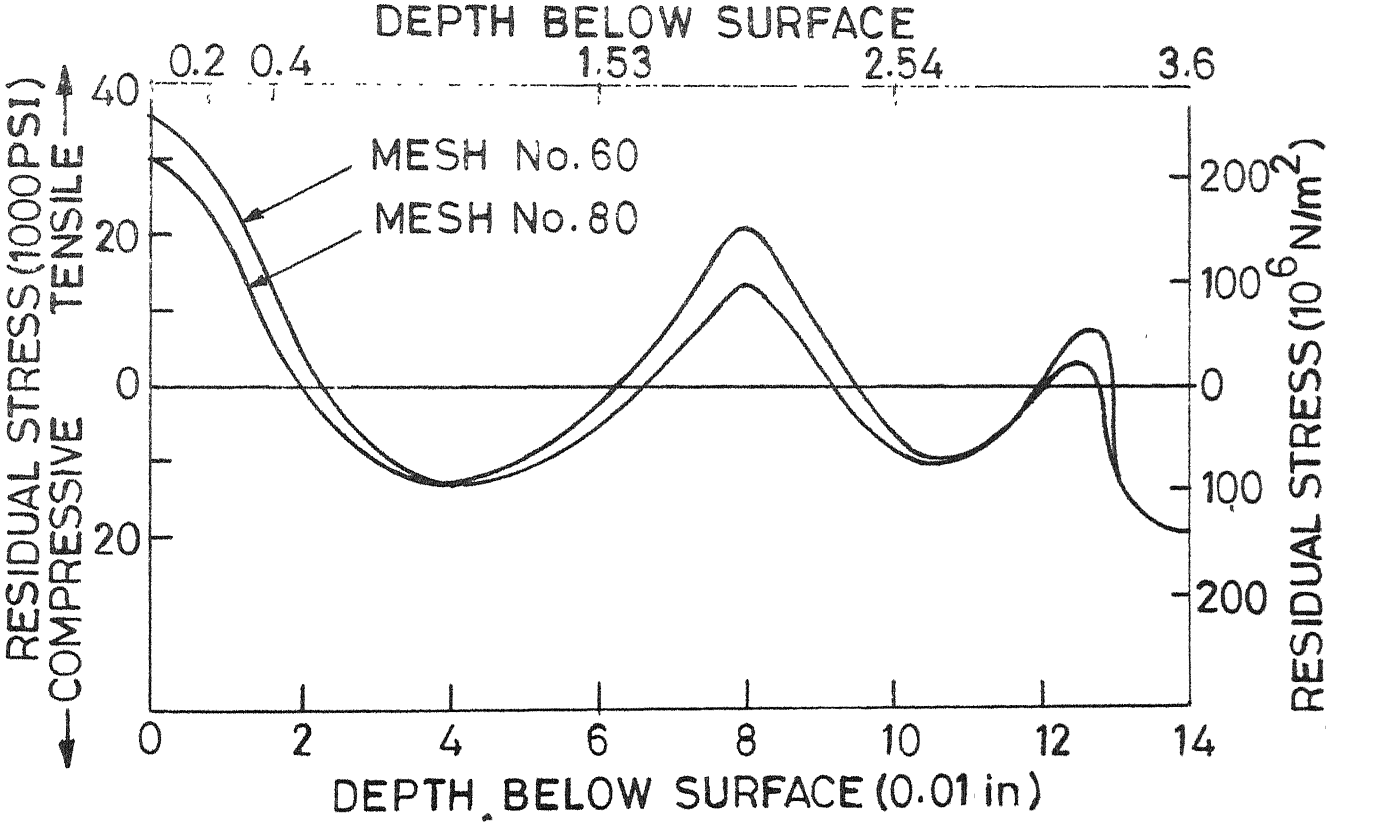

FIG. 23 EFFECT OF GRAIN SIZE ON RESIDUAL STRESS DISTRIBUTION FOR SETS 7,16

A 54918

Date Slip A 54918

This book is to be returned on the date last stamped.

CD 6.72.9

ME-1978-M-BAL-RES